

Galaxy Spiral Arm Count vs. Concentration and Mass: A First Look with Euclid

BEVERLY J. SMITH,¹ SYDNE BERGNER,¹ MARK L. GIROUX,¹ AND CURTIS STRUCK²

¹*Department of Physics and Astronomy, East Tennessee State University, Johnson City TN 37614*

²*Iowa State University, Department of Astronomy, Ames IA*

ABSTRACT

Using catalogued information from Euclid Quick Data Release 1, we compare 2-armed and 3-armed spiral galaxies as classified by the Euclid Zoobot software. Two-armed galaxies have larger concentrations, lower stellar masses (M^*), and lower star formation rates (SFRs) on average than 3-armed galaxies. For a given M^* , 2-armed galaxies have larger concentrations than 3-armed galaxies. These trends have been seen before in nearby galaxies; with Euclid we extend the patterns to redshifts $z = 0.4 - 1$. Two-armed galaxies have lower SFRs because they have lower masses; at fixed M^* , 2-armed and 3-armed galaxies have similar SFRs. We see a bend in the concentration-log M^* relation for 2-armed galaxies at $M^* \approx 10^{10.3} M_\odot$. Above this mass, 2-armed galaxies show significantly larger concentrations than their lower mass counterparts. The observed concentrations of 2-armed galaxies decrease with increasing redshift, perhaps from morphological K-corrections and resolution differences. About 60% – 70% of Euclid spirals are 2-armed, and about 15% – 20% are 3-armed. One-armed galaxies are rare, with low masses compared to 2-armed spirals. We compare these statistics with Galaxy Zoo Sloan Digital Sky Survey arm counts at low z , and tentatively with JWST at higher z . We discuss these results in terms of theoretical models of spiral arm generation and evolution, and compare with statistics of grand design, multi-armed, and flocculent galaxies. There is a need for more quantitative measurements of arm structure beyond arm counts provided by the Zoobot/Galaxy Zoo or the three standard arm classes.

Keywords: Spiral galaxies (1560) — Spiral arms (1559) — Galaxy classification systems (582) (-)– Galaxy evolution (594) — Galaxy structure (622)— Galaxy bulges (578)

1. INTRODUCTION

Spiral galaxies can be divided into classes based on the number of arms and the structure of the arms. Grand design spiral galaxies have two long continuous arms, multi-armed galaxies have three or more relatively long arms, and flocculent galaxies have many short arm fragments (Elmegreen et al. 2011; Buta et al. 2015). Multi-armed spirals sometimes have two arms in their interior, which branch into four or more arms further out in the disk (Elmegreen & Elmegreen 1982; Grosbøl et al. 2004; Buta et al. 2015; Smith et al. 2024; Wei et al. 2024). Our own Milky Way is multi-armed, with four outer arms (Vallée 2016; Reid et al. 2019) possibly branching from two arms in the interior (Minniti et al. 2021; Xu et al. 2023; Kong et al. 2025). The number of arms in a galaxy and their lengths may reflect both the underlying mass distribution of the galaxy as well as its dynamical history.

Observationally, the number of arms correlate with other properties of the galaxies. Grand design galaxies tend to have earlier Hubble types and larger concentrations than multi-armed galaxies with the same stellar mass (Elmegreen & Elmegreen 1982; Bittner et al. 2017; Yu & Ho 2020; Smith et al. 2024). Grand design and multi-armed galaxies populate different regions in a concentration-stellar mass diagram, with grand design galaxies tending to have larger concentrations but smaller stellar masses on average (Smith et al. 2024). Flocculent galaxies tend to have lower masses (Bittner et al. 2017), lower luminosities (Elmegreen & Elmegreen 1982; Ann & Lee 2013), smaller sizes (Elmegreen & Elmegreen 1987), and later Hubble types (Elmegreen et al. 2011; Ann & Lee 2013) than other spirals. These observational trends provide clues to the processes that generate and maintain spiral arms in galaxies.

Multiple mechanisms may contribute to the spiral patterns observed in galaxies. Gravitational instabilities in isolated differentially-rotating disks can produce transient but recurring spiral patterns (Goldreich & Lynden-Bell 1965), which can be enhanced by galactic shear via swing amplification (Julian & Toomre 1966; Sellwood 2012; Baba et al. 2013; D’Onghia et al. 2013; Dobbs & Baba 2014; Michikoshi & Kokubo 2018). Tidal interactions between galaxies can also induce spiral patterns in disks (Toomre & Toomre 1972; Byrd & Howard 1992; Oh et al. 2008; Dobbs et al. 2010; Struck et al. 2011; Oh et al. 2015). Galactic bars may drive spiral patterns (Sanders & Huntley 1976; Kormendy & Norman 1979; Athanassoula 1980; Salo et al. 2010). Spiral density waves (Lin & Shu 1964, 1966; Shu 2016) may be present in some galaxies, and may be long-lived under some circumstances (Lin & Bertin 1985; Bertin et al. 1989a,b; Saha & Elmegreen 2016).

According to classical spiral density wave theory, a dense concentrated bulge may stabilize a two-armed spiral density wave pattern and extend its lifetime (Lin & Bertin 1985; Bertin et al. 1989a,b) an idea supported by numerical simulations (Saha & Elmegreen 2016). This is compatible with the tendency of grand design galaxies to have large bulges. The morphologies of flocculent galaxies can be reproduced by simulations of stochastic gravitational collapse in differentially-rotating disks (D’Onghia et al. 2013). These kinds of models can also produce spiral patterns like those seen in multi-armed galaxies, if the simulation has a large disk mass compared to the dark matter surface density (D’Onghia et al. 2013; Fujii et al. 2018). In these models, the arms tend to be long and well-defined. In contrast, simulations with proportionally smaller disk/halo mass surface densities tend to produce flocculent spirals (D’Onghia et al. 2013; Fujii et al. 2018). Models with high star formation rates (SFRs) and high stellar feedback are more likely to produce flocculent morphologies (Dobbs et al. 2018). Simulations of stochastic production of spiral arms in isolated galaxies can also produce transient 2-armed patterns if they have large disk/halo masses, large bulges, and high shear rates (Grand et al. 2013; D’Onghia 2015; Michikoshi & Kokubo 2018; Patsis & Okalidis 2025). The spiral patterns created by bar-driving models tend to be 2-armed (Athanassoula 2012), or 2-armed in the interior, branching to 4-armed in the outskirts (Grosbøl et al. 2004). Observationally, barred galaxies tend to have two arms in the inner region, branching to form multiple arms further out (Wei et al. 2024). Branching may be associated with orbital resonances (Patsis et al. 1997; Elmegreen & Elmegreen 1995; Chakrabarti et al. 2003). Barred galaxies tend to have stronger spiral arms than unbarred galaxies (Salo et al. 2010), supporting the idea of bar driving. However, this correlation may simply mean that conditions that favor bars also favor strong arms (Díaz-García et al. 2019).

Simulations of spirals produced by galaxy interactions generally have grand design morphologies, but branching of the arms is sometimes seen (Oh et al. 2015). One-armed spirals, although rare, may also be linked to galaxy interactions (Thomasson et al. 1989; Casteels et al. 2013). The grand design spirals present in M51-like galaxies are likely driven by the interaction (Dobbs et al. 2010), but whether the spirals in all 2-armed galaxies were produced by interactions is a matter of debate. Observationally, spiral galaxies in clusters are more likely to be 2-armed compared to field galaxies (Yeoun-Gyu Choi & Ann 2011; Ann 2014; Hart et al. 2016; Smith et al. 2022). However, cluster spirals are also more likely to have large bulges than field spirals (Goto et al. 2003; Weinmann et al. 2009; Smith et al. 2022). and galaxies with larger bulges are more likely to be 2-armed. When comparing galaxies with similar concentrations, Smith et al. (2022) found similar arm counts in cluster and field galaxies. They concluded that the primary factor that determines the number of arms is the concentration rather than the environment.

The spiral arms in zoom-in hydrodynamical cosmological simulations of Milky Way-like galaxies in Local Group-like environments or more isolated locations have been studied by Quinn et al. (2025) and Ghosh & D’Onghia (2025). Quinn et al. (2025) find that 2-armed patterns dominate the stellar morphologies of their model galaxies. In some cases, they can match a specific 2-armed pattern to a particular minor merger, indicating that weak tidal interactions play a role even in relatively low density environments. However, they cannot link all 2-armed patterns to tidal interactions, suggesting that stochastic collapse may create some 2-armed morphologies. Quinn et al. (2025) note that their model galaxies host multiple spiral patterns at once, and suggest that more than one mechanism may be needed to explain the observed structures.

In the local Universe, the distribution of spiral galaxies in a concentration-log M^* plane shows a bend, with many more high concentration galaxies above $M^* = 10^{10} M_{\odot}$ than below (Luo et al. 2020; Smith et al. 2022). This bend is also visible in plots of Σ_1 , the surface brightness in the inner kpc, vs. M^* (Luo et al. 2020). The rapid increase in concentration above $M^* = 10^{10} M_{\odot}$ corresponds to a sudden increase in surface brightness. Luo et al. (2020) suggest that this bend is caused by the growth of classical bulges at high stellar masses. A classical bulge is rounder in appearance and populated by stars in approximately random orbits, in contrast to more flattened pseudo-bulges which show a net rotation (Kormendy & Kennicutt 2004; Athanassoula 2005; Neumann et al. 2017; Gao et al. 2020).

The bend in the Σ_1 vs. $\log M^*$ relation for galaxies has been detected out to $z \sim 3$ (Barro et al. 2017). The bend may be a product of the non-simultaneous growth of the bulge, the halo, and the stellar disk due to mergers, gas accretion, star formation, feedback, and quenching over the history of the Universe (Luo et al. 2020; Barro et al. 2017; Cattaneo et al. 2025). In the local Universe, the bend in the C-log M^* diagram is particularly noticeable when the sample is limited to grand design galaxies; the majority of the high concentration, high mass spiral galaxies are grand design, while high mass galaxies with lower concentrations tend to be multi-armed (Smith et al. 2024).

Whether the local relations between the number of arms, the concentration, and the stellar mass of spiral galaxies extend to higher redshifts is uncertain. With Hubble Space Telescope rest-frame optical images, only about 10% of galaxies at $z \sim 1.5$ can be identified as spirals (Margalef-Bentabol et al. 2022), but the higher sensitivity and better resolution imaging of JWST indicates larger percentages of spirals. Kuhn et al. (2024) report a spiral fraction of about 40% at $z \sim 0.75$; they conclude that the fraction drops to 30% at $z \sim 3$ after they correct for resolution effects. In another JWST study of $10^{10} M_\odot \leq M^* < 10^{11.4} M_\odot$ galaxies, Espejo Salcedo et al. (2025) conclude that the fraction of spirals decreases from 55% at $z \sim 1$ to 20% at $z \sim 2.25$. Espejo Salcedo et al. (2025) classify about 2/3rd of the spirals in their sample as 2-armed, and approximately 1/3 as 3-armed. For comparison to these numbers, Hart et al. (2016) use Galaxy Zoo 2 citizen scientist classifications (Willett et al. 2013) to estimate that 64% of spirals with $M^* \geq 10^{10.6} M_\odot$ in the local Universe are 2-armed, and 18% are 3-armed. Espejo Salcedo et al. (2025) conclude that the fraction of 2-armed galaxies at $z \sim 1$ is similar to the Hart et al. (2016) local values, but the numbers of 3-armed galaxies at high redshift is enhanced relative to local galaxies. Espejo Salcedo et al. (2025) suggest that the larger gas fractions, enhanced turbulence, and higher star formation rates (SFRs) at higher redshifts favor 3-armed morphologies. This idea is supported by simulations by Bland-Hawthorn et al. (2024), which show that gas-rich turbulent disks can produce transient 3-armed patterns in their inner regions.

To investigate the relations between arm number, concentration, stellar mass, and redshift, it would be helpful to study galaxies in the intermediate redshift range of $0.2 - 1$ to connect trends seen in the local Universe with those at higher redshifts. To this end, we present a first attempt to observationally determine the spiral-arm-number-concentration- M^* relation for galaxies with $0.2 < z < 1$ using Euclid satellite (Euclid Collaboration: Mellier et al. 2025) galaxy catalogs (Euclid Collaboration: Romelli et al. 2025; Euclid Collaboration: Walmsley et al. 2025). In Section 2, we describe the Euclid dataset and our sample selection, and investigate the fraction of spirals that are 2-armed and 3-armed as a function of redshift. We explore the relations between concentration, mass, and SFR for 2-armed vs. 3-armed galaxies in Section 3. In Section 4, we discuss the 1-armed galaxies. In Section 5, we compare with earlier studies and discuss the implications of our results. A summary is given in Section 6. As in the earlier Euclid papers, we assume the Planck 2016 flat Λ CDM cosmology with $H_0 = 67.74 \text{ km s}^{-1} \text{ Mpc}^{-1}$, $\Omega_m = 0.3089$, and $\Omega_\Lambda = 0.6911$ (Planck Collaboration: Ade et al. 2016).

2. DATA AND SAMPLE

2.1. Euclid Data and Catalogs

The Euclid satellite (Euclid Collaboration: Mellier et al. 2025) is currently mapping the sky at both visible and near-infrared wavelengths. In this paper, we will focus on images obtained with the Visible Imager (VIS), which uses a broadband optical I_E filter ($0.53 - 0.92 \mu\text{m}$) and provides a FWHM spatial resolution of $0''.18$ and a pixel size of $0''.1$ (Euclid Collaboration: Cropper et al. 2025). The Euclid Quick Release 1 (Q1) data release covers a total of 63.1 degree^2 , in three fields: the Euclid Deep Field North (EDF-N), Euclid Deep Field South (EDF-S), and Euclid Deep Field Fornax (EDF-F) (Euclid Collaboration: Aussel et al. 2025). The Euclid Q1 data release ‘merged’ MER catalog (Euclid Collaboration: Romelli et al. 2025) contains about 29 million sources. The MER catalog provides fluxes, the spatial area of the galaxy in the segmentation map (`segmentation_area`), Sérsic fits to the radial light profiles, estimates of the concentration, and many other parameters. The concentration is defined as $C = 5 \log_{10} (r_{80}/r_{20})$ (Kent 1985; Conselice 2014).

Using both Euclid and ground-based data, photometric redshifts and physical parameters were derived for about 26 million of the MER catalog galaxies, and tabulated in the PHZ catalog (Euclid Collaboration: Tucci et al. 2025). The PHZ catalog provides two estimates of redshifts: photometric redshifts (PHZ_MEDIAN) from the template-fitting *Phosphoros* software, and redshifts inferred from spectral energy distribution (SED) fits for the physical parameters of the galaxies obtained with the Nearest-Neighbour Photometric Redshifts (NNPZ) software. The PHZ catalog parameters PHZ_PP_MEDIAN_Z and PHZ_PP_MODE_Z are the median and mode of the NNPZ redshifts. The NNPZ SED-fitting routine also provides estimates of the stellar mass and SFR. Euclid Collaboration: Tucci et al.

(2025) compared the PHZ redshifts with spectroscopic redshifts, and concluded that the accuracy of the photometric redshifts, defined as the median $|z_{\text{phot}} - z_{\text{spec}}|$, is about 2%, while the precision, as measured by the normalized median absolute deviation, is 0.03 for $I_E < 23$. They find an outlier fraction of 10% in the north and 16% in the south, where outliers are defined as galaxies for which the photometric redshift is off by more than 0.15.

Euclid Collaboration: Walmsley et al. (2025) used the Zoobot galaxy morphology foundation model to derive morphological parameters for a subset of 380,111 of the Euclid galaxies in the MER catalog. The Zoobot software mimicked Galaxy Zoo 2 citizen scientist responses to a set of questions about each galaxy. These questions include whether the galaxy is smooth or featured, whether it is an edge-on disk, and whether a spiral pattern is visible. If those questions are answered positively, then citizen scientists were asked how many arms were present. The Zoobot catalog provides synthetic ‘vote fractions’ for each galaxy in the sample, mimicking the expected responses that a set of random citizen scientist volunteers would have selected for each galaxy. These vote fractions were not corrected for redshift classification bias, so are equivalent to the ‘raw’ vote fractions used by **Hart et al. (2016)**.

The Zoobot was pre-trained using Euclidized Hubble Space Telescope images, then trained using Galaxy Zoo volunteer annotations of preliminary Euclid Wide Survey images. This Euclid training set was selected based on the criteria `segmentation_area > 1200 pixels OR $I_E < 20.5$ AND segmentation_area > 200 pixels`. In the production of the morphological catalog, the sample was extended to fainter ($I_E < 23$) galaxies, but with a `segmentation_area` limit of `> 700`. This means that the software was applied to some galaxies that were fainter than the original training set. To exclude artifacts, **Euclid Collaboration: Walmsley et al. (2025)** limited their catalog to galaxies with the MER parameter `vis_det` set to 1 (i.e., the object was detected in the visible), and the `spurious_prob` parameter set to `< 0.2`.

2.2. Sample Selection

We started with the **Euclid Collaboration: Walmsley et al. (2025)** Euclid morphology catalog of 380,111 galaxies (**Walmsley et al. 2025**). We cross-correlated with the Dark Energy Spectroscopic Explorer (DESI) Data Release 1 spectroscopic redshift catalog (**DESI Collaboration: Abdul-Karim et al. 2025**) using a $2''$ offset, and found 18,673 matches. When available, we used the DESI spectroscopic redshift in the following analysis; otherwise, we used the NNPZ photometric redshift `PHZ_PP_MEDIAN_REDSHIFT`. Following **Euclid Collaboration: Quilley et al. (2025)**, we eliminated objects with axis ratio ≤ 0.05 (i.e., `seraic_sersic_vis_axis_ratio` parameter ≤ 0.05), since those are likely artifacts, and restricted the sample to galaxies with reliable physical parameters in the PHZ catalog (`phys_param_flags = 0`). As in **Euclid Collaboration: Quilley et al. (2025)**, we eliminated galaxies with large differences between the two photometric determinations of redshift, only retaining galaxies with $|\text{PHZ_PP_MEDIAN_Z} - \text{PHZ_MEDIAN}| < 0.2$ and $|\text{PHZ_PP_MEDIAN_Z} - \text{PHZ_PP_MODE_Z}| < 0.2$ unless a spectroscopic redshift is available. To remove spurious and compact sources, we required `DET_QUALITY_FLAG < 4` and `MUMAX_MINUS_MAG > -2.6`, as in **Euclid Collaboration: Tucci et al. (2025)**. We also excluded galaxies with PHZ specific SFRs (sSFRs) $> 10^{-8.2} \text{ yr}^{-1}$, as their parameters may be unreliable (**Euclid Collaboration: Tucci et al. 2025**). In our final analysis, we only included galaxies with both concentration and stellar mass available from the PHZ catalog, and Sérsic index from the MER catalog. We also eliminated objects with unreliable physical parameters by requiring the stellar mass to be less than $10^{12} M_\odot$ and the concentration to be less than 20.

The Euclid morphological catalog (**Euclid Collaboration: Walmsley et al. 2025**) only provides Zoobot spiral arm count vote fractions for galaxies with $p_{\text{featured}} \times p_{\text{notedge-on}} \times p_{\text{spiral}} > 0.5$, where p_{featured} , $p_{\text{notedge-on}}$, and p_{spiral} are the Zoobot’s estimated vote fractions for the questions about smoothness vs. features/disk, non-edge-on disks, and the presence of a spiral pattern, respectively. We limited our sample to spiral galaxies with effective radii (half-light radii) greater than or equal to $0''.5$, as determined by the Sérsic-fitting routine (parameter `seraic_sersic_vis_radius`). This radius is $3\times$ the FWHM resolution, sufficient for reasonable morphological study. This requirement only eliminates a few galaxies that meet the other criteria. Limiting the initial sample to $0.15 \leq z \leq 1.2$, a total of 32,974 galaxies meet the above criteria; 11,514 of these are in the EDF-N field, 15,468 in the EDF-S field, and 5992 in the EDF-F field. Of the 32,974 galaxies in our initial sample of spirals, 2172 have DESI spectroscopic redshifts. The full set of criteria used to select our initial sample of spiral galaxies is given in Table 1.

2.3. The Fraction of Spirals with Different Arm Counts, as a Function of Redshift

We initially assigned each galaxy in the spiral sample to one of the following six classes: 1-armed, 2-armed, 3-armed, 4-armed, 5+-armed, or ‘can’t tell the number of arms’, by placing them in the class for which the Zoobot gave the highest vote fraction. To determine how the fraction of spiral galaxies of each class changes with redshift, we need to

Table 1. Galaxy Sample Selection Criteria

Catalogue	Parameter(s) and Criteria	Source	Notes
MER	segmentation_area > 1200 pix	Euclid Collaboration: Walmsley et al. (2025)	
OR			
MER	($I_E < 20.5$ AND segmentation_area > 200 pix)		
MER	vis_det = 1	Euclid Collaboration: Walmsley et al. (2025)	
MER	spurious_prob < 0.2	Euclid Collaboration: Walmsley et al. (2025)	
PHZ	phz_param_flags = 0	Euclid Collaboration: Quilley et al. (2025)	
PHZ	PHZ_PP_MEDIAN_Z - PHZ_MEDIAN < 0.2	Euclid Collaboration: Quilley et al. (2025)	1
PHZ	PHZ_PP_MEDIAN_Z - PHZ_PP_MODE_Z < 0.2	Euclid Collaboration: Quilley et al. (2025)	1
MER	spurious_flag = 0	Euclid Collaboration: Quilley et al. (2025)	
MER	sersic_sersic_vis_index < 5.45	Euclid Collaboration: Quilley et al. (2025)	
MER	sersic_sersic_vis_axis_ratio >= 0.05	Euclid Collaboration: Quilley et al. (2025)	
MER	mumax_min_mag_x/y ≥ -2.6	Euclid Collaboration: Tucci et al. (2025)	
MER	det_quality_flag < 4	Euclid Collaboration: Tucci et al. (2025)	
PHZ	phz_flag = 0	Euclid Collaboration: Tucci et al. (2025)	
PHZ	log sSFR < -8.2	Euclid Collaboration: Tucci et al. (2025)	
PHZ	phz_pp_median_stellarmass available	This work	
PHZ	phz_pp_median_sfr available	This work	
PHZ	phz_pp_median_stellarmass < 12	This work	
MER	concentration < 20	This work	
MER	sersic_sersic_vis_radius ≥ 0.5	This work	
MER	$p_{\text{featured}} \times p_{\text{notedge-on}} \times p_{\text{spiral}} > 0.5$	Euclid Collaboration: Walmsley et al. (2025)	
	$0.15 \leq z \leq 1.2$	Our initial spiral sample	
	$\log(M^*/M_\odot) \geq 10.6$	Our mass-limited spiral sample	
morph	spiral-arm-count_2.fraction ≥ 0.8	Our highly reliable 2-armed sample	
morph	spiral-arm-count_3.fraction ≥ 0.5	Our highly reliable 3-armed sample	
	$8.5 \leq \log(M^*/M_\odot) < 12$	Our highly reliable samples	

¹Unless spectroscopic redshift available from DESI.

take into account completeness as a function of mass, which depends upon redshift. As we show below (Section 3.2), at $z = 0.2$ the sample is about 90% complete to $\log(M^*/M_\odot) = 10.0$. By a redshift of $z = 0.5$, the sample is only 50% complete at $\log(M^*/M_\odot) = 10.6$. In the following discussion of the fraction of spirals in the different classes as a function of redshift, we only include galaxies with $\log(M^*/M_\odot) \geq 10.6$. We call this the mass-limited spiral sample. Note, however, that at redshifts greater than 0.5 this mass-limited sample is somewhat incomplete even with a $\log(M^*/M_\odot) \geq 10.6$ limit. The total number of galaxies in the mass-limited sample is 10,820 galaxies.

For this mass-limited spiral sample, the fraction of the spiral galaxies in each of these classes (including the ‘can’t-tell’ class) is plotted as a function of redshift in Figure 1. To construct this figure, we divided the galaxies into redshift bins of width $\Delta z = 0.05$ for $0.15 < z < 1.2$. At all redshifts, the majority of the galaxies are placed in the 2-armed category. Ignoring the lowest redshift bin as having poor statistics and averaging over the second and third redshift bins ($0.175 \leq z < 0.275$), the percentage of galaxies with $\log(M^*/M_\odot) \geq 10.6$ classified by the software as 1-armed/2-armed/3-armed/4-armed/5+-armed/cant-tell are $0.5 \pm 0.4\%$, $54 \pm 3\%$, $12 \pm 2\%$, $0.05 \pm 0.4\%$, $11 \pm 2\%$, and $22 \pm 2\%$, respectively. The Zoobot places almost 1/4th of the galaxies at $z \sim 0.2$ in the ‘can’t-tell’ class. These ‘can’t-tell’ galaxies may be a combination of flocculent galaxies and multi-armed galaxies for which the arm counts are unclear. The fraction of galaxies listed as ‘can’t-tell’ drops off with redshift, perhaps because at higher redshifts the software is no longer able to discern a spiral pattern, so the galaxies are not included in the spiral sample.

In Figure 1, we provide curves for the EDF-N, EDF-S, and EDF-F fields separately, in addition to values for the sample as a whole. Around $z = 0.2$, there is considerable scatter from field to field. At $z = 0.2$, the EDF-N field has a much higher fraction of 2-armed galaxies compared to the other fields. A comparison of the Euclid photometric redshifts with published spectroscopic redshifts showed that in the EDF-N field, the outliers cover a spread in redshift, but in the EDF-S and EDF-F fields, a large fraction of the outliers were at $z_{phot} = 0.2 - 0.3$ and $z_{spec} = 0.5 - 0.8$ (Euclid Collaboration: Tucci et al. 2025). This means that the $z = 0.2$ statistics are less reliable for EDF-S and EDF-F than for EDF-N. These redshift errors may contribute to the scatter seen at $z \sim 0.2$ in Figure 1. Since about 3/4th of the sample galaxies are in the southern and Fornax fields, the overall statistics at $z = 0.2$ may be skewed by these outliers.

In the statistics given below, to be consistent with Hart et al. (2016) we exclude galaxies identified as ‘can’t-tell’ from the quoted fractions. Excluding ‘can’t-tell’ galaxies, $65 \pm 2\%$ of the $0.175 \leq z < 0.275$ spirals are placed in the 2-armed class and $15 \pm 2\%$ in the 3-armed class. These percentages are uncertain, however, because of the field-to-field scatter at $z = 0.2$ noted above. Between $z = 0.20$ and 0.25 the percentage of 2-armed galaxies in the full sample increases from $57 \pm 5\%$ to $69 \pm 3\%$, but in the EDF-N field, the percentage drops from $76 \pm 10\%$ to $66 \pm 7\%$.

Over a larger redshift range, there is a clear increase with redshift in the fraction of galaxies classified as 2-armed. The percentage of 2-armed galaxies increases from $\sim 65\%$ at low redshifts to 84% at $z \sim 0.6$. The fraction of spirals placed in the 3-armed category is about 15 - 20% from $0.2 \leq z < 0.4$, then gradually drops to about 15% at $z \sim 0.6 - 0.8$. The percent of 4-armed galaxies is about 1 - 2% at $z \sim 0.2$ and drops to $\sim 0.5\%$ at $z \sim 0.6$. The fraction of galaxies classified as 5+-armed is substantial at $z \sim 0.2$ (21%), but drops quickly at higher redshifts, falling to about 6% at $z = 0.4$ and 1% at $z = 0.6$. In contrast to the 3-armed, 4-armed, and 5+-armed fractions, the fraction of 1-armed galaxies increases slightly with redshift, though it remains small. It is $0.5 \pm 0.4\%$ at $0.175 \leq z < 0.275$, $1.1 \pm 0.2\%$ at $0.4 \leq z \leq 0.6$, and $1.6 \pm 0.3\%$ at $0.8 \leq z < 1$.

The datapoints in the left panel of Figure 1 are color-coded based on the median raw vote fraction for galaxies in that class. For galaxies that we classify as 2-armed, the median vote fraction for two arms is typically 0.6 - 0.7, i.e., a majority of the votes. In contrast, for the galaxies in the other classes, the median vote fraction in their selected class is typically less than 0.5, meaning that, although a plurality of the votes placed them in their class, it was not the majority.

The redshift trends in the fractions of galaxies in each class are likely caused at least in part by classification bias. At higher redshifts, viewers may undercount the number of arms, causing the dramatic drop in 5+-armed systems between $z = 0.2$ and $z = 0.6$. For more nearby galaxies, one might be able to see further out in the disk where branching of arms may occur, giving a higher arm count. More generally, multi-armed galaxies may be mis-identified as 2-armed at higher redshifts. Furthermore, at higher redshifts the spiral patterns in multi-armed and flocculent galaxies may be hard to see, thus such galaxies are more likely to be omitted from the spiral dataset at higher redshifts.

For comparison to these numbers, Hart et al. (2016) found bias-corrected percentages (excluding ‘can’t-tell’ galaxies) of 1-armed/2-armed/3-armed/4-armed/5+-armed spiral galaxies of 5%/64%/18%/6%/7% for galaxies with $\log(M^*/M_\odot) \geq 10.6$ in the $0.03 < z < 0.085$ range. Their percentages of 2-armed and 3-armed agree well with ours at $0.2 < z < 0.4$, showing good consistency between the Euclid Zoobot values and the SDSS Galaxy Zoo 2 data. However, the Euclid Zoobot finds a higher fraction of 5+-armed galaxies and a lower fraction of 1-armed and 4-armed galaxies at $z = 0.2$ than Hart et al. (2016) found for SDSS galaxies at $z = 0$. The difference in the fraction of 5+-armed galaxies may be a consequence of the excellent spatial resolution of Euclid. At a redshift of 0.2 the Euclid spatial resolution of $0''.16$ corresponds to a spatial scale of 0.53 kpc, while at a redshift of 0.03, the lower edge of the SDSS range studied by Hart et al. (2016), the SDSS spatial resolution of $1''.3$ corresponds to a spatial scale of 0.79 kpc. In Section 5.4, we compare our Euclid statistics with other studies besides Hart et al. (2016).

The strong trends with redshift indicate that classifier bias is present in the raw Euclid Zoobot vote fractions. As a first attempt to disentangle the effects of observer bias and galaxy evolution in the observed trends, we will make a simple assumption. JWST observations find that about $\sim 60\%$ of spirals with $10^{10} M_\odot \leq M^* < 10^{11.4} M_\odot$ are 2-armed at $z = 1$ (Espejo Salcedo et al. 2025), similar to the Hart et al. (2016) SDSS percentage and also similar to the 65% we find from Euclid at $z \sim 0.2$. We will therefore naively assume that the fraction of 2-armed galaxies remains constant with redshift at 65% for $0.2 < z < 1$. This is an over-simplistic assumption, since the spiral structures of galaxies may evolve significantly between $z = 1$ and $z = 0.2$. However, given the apparent agreement for 2-armed galaxies between SDSS, JWST, and $z \sim 0.2$ Euclid, we will assume that the fraction of 2-armed spirals is constant, and then investigate how the fractions for the other classes change.

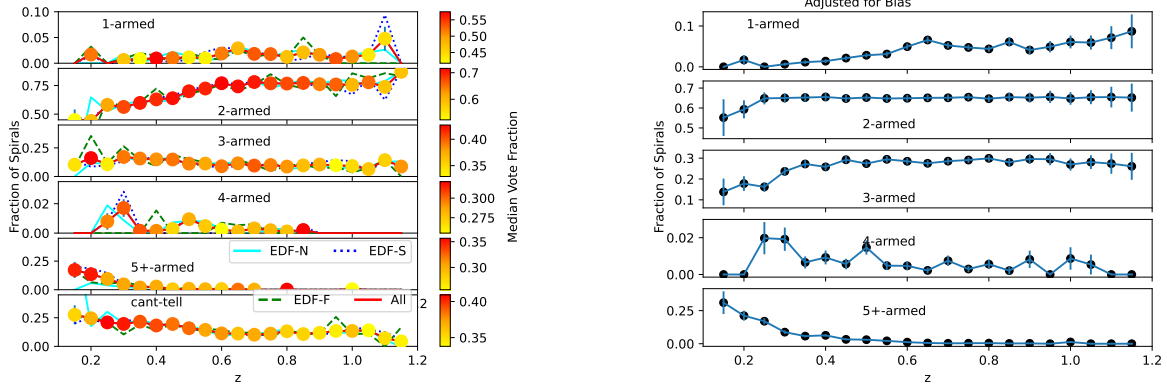


Figure 1. Left: The fraction of $M^* \geq 10^{10.6} M_{\odot}$ spiral galaxies that are placed in the various arm count categories, as a function of redshift. These fractions were calculated using the raw vote fractions from the Zoobot, and include the ‘can’t tell’ class. The solid red line and colored points are for the full set of data; the cyan solid line, dotted blue line, and green dashed line are for EDF-N, EDF-S, and EDF-F, respectively. The datapoints are color-coded from yellow to red based on the mean vote fraction for that datapoint, as shown by the individual colorbars to the right. Right: The fraction of $M^* \geq 10^{10.6} M_{\odot}$ galaxies that are placed in the arm count categories, after correction for bias. The ‘can’t-tell’ galaxies are not included in the statistics shown on the right. For these bias correction, the fraction of galaxies identified as 2-armed is fixed at 65%, and the 2-armed vote fractions are scaled down from their raw values accordingly.

At each redshift bin, for each galaxy we multiply the Zoobot vote fractions for 2-arms by a scale factor less than 1, to account for the apparent observer bias. We empirically determine what this scale factor is at each redshift by requiring the fraction of 2-armed spirals to remain fixed at 65%. To be consistent with Hart et al. (2016), we have excluded galaxies in the ‘can’t-tell’ class from the bias correction. The ‘can’t-tell’ galaxies were excluded from the sample, and the bias correction was done on the remaining galaxies. The application of this scale factor will move some of the galaxies previously listed as 2-armed to other categories. For a given redshift, we use the same scale factor for galaxies of all masses, rather than binning the galaxies further by mass and size as done by Willett et al. (2013). The corrected vote fractions as a function of redshift are displayed in the right panel of Figure 1. In contrast to the left panel of Figure 1, the right panel excludes the can’t-tell galaxies.

Since typical vote fractions for 3-armed galaxies are usually higher than for 4-armed or 5+-armed systems (left panel, Figure 1), when the vote fractions for 2-armed are lowered in the correction process, galaxies are more likely moved from the 2-arm class to the 3-arm class. Therefore, by requiring the 2-arm fraction to be fixed with redshift, we increase the 3-arm fraction at higher redshift. In the corrected plots, the 3-arm fraction rises quickly from 20% at $z = 0.2$ to 30% at $z = 0.3$, and then remains constant at about 30% to $z = 1$. This rapid rise in the corrected fraction of 3-armed galaxies between $z = 0.2$ and $z = 0.3$ is probably artificial, perhaps caused by the systematic problems with the photometric redshifts at $z = 0.2$ which cause the field-to-field variations. Many of the galaxies reclassified as 3-armed by the bias correction may actually be 4-armed or 5+-armed.

Another possible artifact in the corrected-for-bias plots is the increase in the fraction of galaxies classified as 1-arm between $z = 0.2$ and $z = 1$. As shown in the left panel of Figure 1, the median vote fractions for galaxies selected as 1-armed are relatively high compared to the 4-armed and 5+-arm classes. Although the fraction of galaxies selected as 1-armed is low, less than 3%, galaxies that are selected as 1-armed tend to have relatively high vote fractions for 1-armedness. This means that when galaxies are not moved to the 3-armed class by the bias correction, they tend to be moved to the 1-arm class.

As a rough estimate of the uncertainties in the corrected fractions of galaxies of each arm count, we calculated bias-corrected fractions assuming the fraction of 2-armed galaxies is constant at 60% or 70% rather than the nominal 65%. These changes caused the corrected fractions for 3-armed galaxies to increase to $\sim 35\%$ or decrease to $\sim 25\%$, respectively.

The above discussion illustrates the large uncertainties in correcting for redshift classification bias in the Euclid database. Even with these large uncertainties, however, it is intriguing that our bias-corrected 3-arm fractions of 30% at $z = 1$ agree well with the JWST fractions at $z = 1$ reported by Espejo Salcedo et al. (2025). This result is

quite uncertain, however, and requires further morphological analysis of the structure of the spiral arms, including an exploration of possible branching in the arms. A more detailed study of redshift classification bias in the Euclid Zoobot database also requires improved photometric redshifts, and is beyond the scope of this study.

2.4. Highly Reliable Samples of 2-Armed and 3-Armed Galaxies

We now further filter our galaxy sets to obtain the purest and most reliable samples of 2-armed and 3-armed galaxies possible. Our ultimate goal is to investigate physical differences between galaxies with different numbers of arms, thus we would like to minimize the numbers of misclassifications. For our final 'highly reliable' sample of 2-armed galaxies, we use the subset of galaxies with raw vote fraction for 2-arms ≥ 0.8 . For our final sample of 'highly reliable' 3-armed galaxies, we limit our sample to galaxies with raw vote fractions for 3-arms ≥ 0.5 . The 2-armed galaxy sample is therefore a purer sample than the 3-armed sample. The less strict selection criteria used for the 3-armed sample is necessitated by the need for a reasonable sample size. As we discuss in Sections 3.3 and 3.4, comparisons of samples of equal purity do not change our conclusions. For both sets of galaxies, we extend the mass range down to $\log(M^*/M_\odot) = 8.5$ to study trends with M^* .

The standard Euclid catalog pipeline background subtraction gives less reliable photometry for large angular size nearby galaxies (Marleau et al. 2025). Furthermore, the Euclid photometric redshift pipeline was designed for galaxies with $z \geq 0.2$ (Euclid Collaboration: Desprez et al. 2020). This means that the photometric redshifts may be less reliable at low z . We therefore limit our sample to $z > 0.2$ in the following analysis. We limit our sample to $z \leq 1$ because of angular size constraints. This gives us 6284 2-armed and 262 3-armed galaxies in our highly reliable subsets. These samples of 2-armed and 3-armed galaxies are compared and contrasted in Section 3.

Likely some of the galaxies classified as 2-armed or 3-armed have fainter arms and branches, and in a more detailed study may be catalogued as 4-armed or multi-armed. In the current study, we assume that the majority of the galaxies in our 2-armed sample have spiral patterns that are dominated by a 2-armed structure, although there may be branches and filaments. Likewise, we assume that the majority of the galaxies we have included in our 3-armed sample fall into the general category of multi-armed galaxies. Smith et al. (2024) investigated Galaxy Zoo 2 (GZ2) arm count statistics for galaxies identified by other methods as either grand design or multi-armed. They found that galaxies in the grand design sample generally had high GZ2 vote fractions as 2-armed. For the multi-armed galaxies in their sample, when they summed the Galaxy Zoo 2 vote fractions for 3-armed, 4-armed, 5+ armed, or 'cannot count arms', the vote fractions were generally greater than 50%. These statistics support our association of our highly reliable 2-armed galaxies with the arm class of grand design galaxies, and our assumption that our highly reliable 3-armed galaxies are mostly multi-armed galaxies.

We also construct a sample of 'highly reliable' 1-armed galaxies, using a vote fraction for 1-arms of ≥ 0.5 . A total of 188 galaxies with $0.2 < z \leq 1$ meet these criteria. These galaxies are discussed further in Section 4. No galaxies have vote fractions for 4-arms or 5+-arms greater than 0.5, so we do not construct 'highly reliable' samples of 4-armed or 5+-armed galaxies.

3. 2-ARMED VS. 3-ARMED GALAXIES

3.1. Magnitude and Redshift Limits

In Figure 2, we plot I_E vs. redshift for our samples of highly reliable 2-armed (left) and 3-armed (right) galaxies. In these plots, we distinguish between galaxies with `segmentation_area` < 1200 pixels and larger galaxies. For a given redshift, galaxies with smaller angular sizes tend to be fainter, as expected. In both panels, the highest density of points occurs at a redshift of ~ 0.3 , but the peak of the distribution for the 2-armed galaxies is at a higher magnitude of ~ 19.9 compared to ~ 19.5 for the 3-armed galaxies (i.e., at $z \sim 0.3$, the distribution of galaxies peaks at a lower luminosity for 2-armed galaxies).

In Figure 2, we overlay (solid horizontal line) the $I_E = 20.5$ limit of the Zoobot training sample for galaxies with `segmentation_area` > 200 pixels. Most of the `segmentation_area` < 1200 galaxies are fainter than this limit. Since the Zoobot software was not trained on small angular size galaxies fainter than this cut-off, classifications of fainter galaxies may be less reliable. For the 2-armed galaxy sample, the distribution of large angular size galaxies extends to about $I_E = 21.5$.

Because of the filtering process described above, our sample is not complete. The completeness of the sample varies in a complicated way with redshift, morphology, angular size, and location in the sky. For example, because of differences in the available ground-based data, the galaxies in the EDF-N field with the largest redshift uncertainties tend to lie

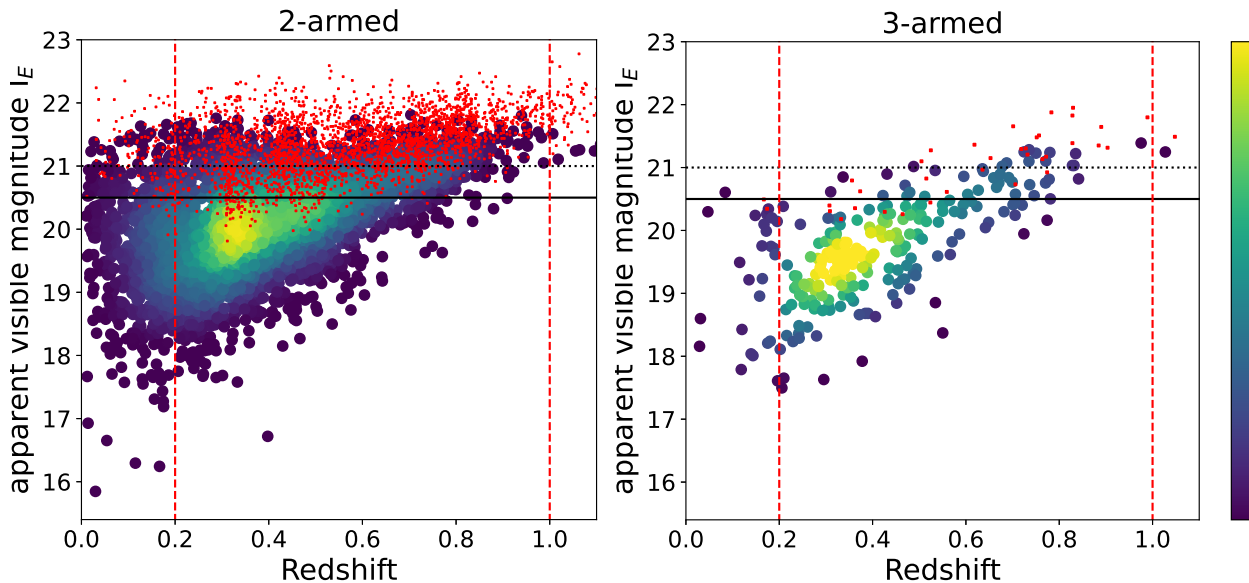


Figure 2. The apparent visible magnitude I_E vs. redshift for our samples of highly-reliable 2-armed galaxies (left) and 3-armed galaxies (right). The red dots represent galaxies with `segmentation_area` < 1200 pixels. For galaxies with larger `segmentation_areas`, the colorbar gives the relative number of galaxies per area on the plot as shown by the colorbar on the right. The horizontal solid black line at $I_E = 20.5$ is the magnitude limit of the Zoobot training sample for `segmentation_area` < 1200 galaxies. The horizontal dotted black line is our estimate of the approximate completeness limit of our samples. As discussed in the text, we limit our final sets of highly reliable 2-armed and 3-armed galaxies to galaxies with $0.2 \leq z \leq 1$, as marked by the vertical red dashed lines. In this plot, we include galaxies outside that redshift range for comparison purposes.

between $0.45 < z < 0.8$, while in the other fields galaxies with highly uncertain redshifts have a larger range of redshift (Euclid Collaboration: Tucci et al. 2025). Although the Euclid Collaboration: Walmsley et al. (2025) morphological catalog includes galaxies to $I_E = 23$, based on Figure 2 we conservatively estimate an approximate completeness limit for our sample of about $I_E = 21$ (dotted horizontal line).

3.2. Stellar Mass vs. Redshift

In Figure 3, we plot stellar mass vs. redshift for our highly reliable samples of 2-armed vs. 3-armed galaxies. As expected, there is a trend in these plots, with larger redshift galaxies tending to be more massive. This result is in part because of incompleteness, with lower mass galaxies being missed at higher redshift. The highest density of datapoints in these plots for both samples of galaxies occurs at around $z = 0.3$, but at a higher stellar mass ($\log(M^*/M_\odot) \sim 10.5$) for the 3-armed galaxies compared to the 2-armed ($\log(M^*/M_\odot) \sim 10.4$).

To calculate completeness limits as a function of stellar mass and redshift, we used the method of Pozzetti et al. (2010): for each galaxy in the sample, we calculated the limiting stellar mass the galaxy would have if its apparent magnitude were equal to the limiting magnitude of the survey. This distribution was then used to calculate the 50% and 90% completeness limit. This method implicitly takes into account the mass/light ratios of the sample galaxies. We find similar completeness limits for the 2-armed and 3-armed galaxy samples at a given redshift (within 0.2 dex).

In Figure 3, at each redshift we mark the 50% and 90% completeness limit as a function of stellar mass assuming our conservative magnitude limit of $I_E < 20.5$. We also mark the 50% completeness mass limit for the more liberal magnitude limit of $I_E < 21$.

3.3. Concentration vs. Stellar Mass

In Figure 4, we plot concentration vs. $\log M^*$ for our highly reliable samples of 2-armed and 3-armed galaxies within four redshift ranges: $0.2 < z \leq 0.4$, $0.4 < z \leq 0.6$, $0.6 < z \leq 0.8$, and $0.8 < z \leq 1$. There are 2361, 2064, 1414, and 485

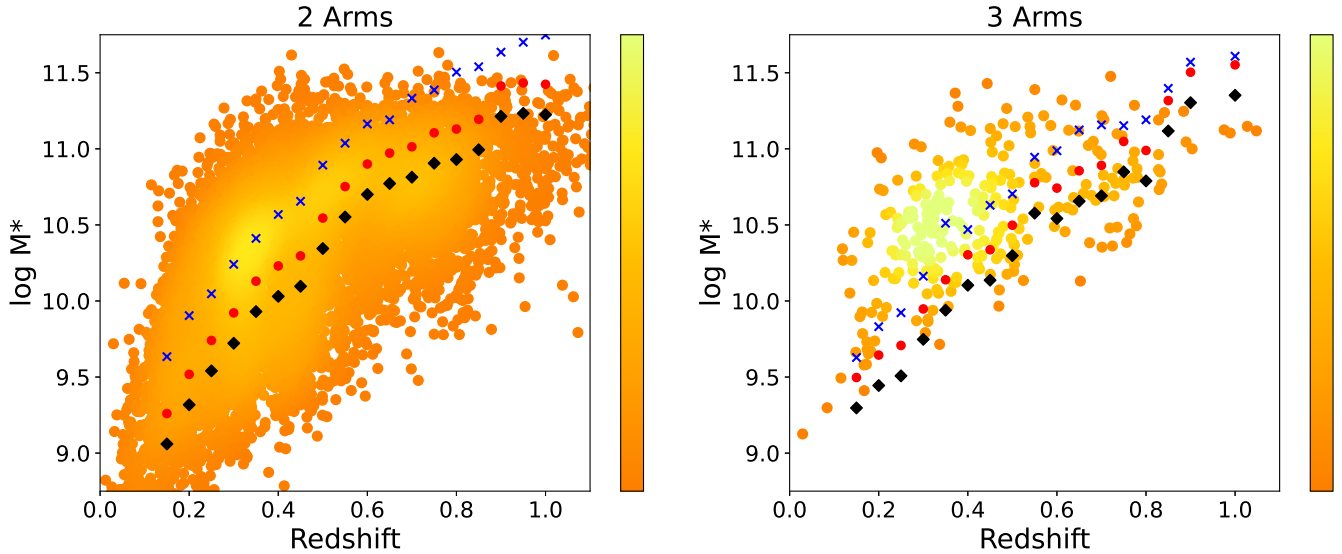


Figure 3. The $\log M^*$ vs. redshift plot for our highly reliable samples of 2-armed (left) and 3-armed galaxies (right). The color scale represents the relative number of galaxies per area on the plot, as shown by the colorbar on the right. The 50% completeness limit assuming a magnitude limit of $I_E = 21$ is plotted as black filled diamonds. The 50% and 90% completeness limits obtained using the stricter limit of $I_E = 20.5$ are plotted as red filled circles and blue crosses, respectively.

2-armed galaxies and 123, 79, 48, and 12 3-armed galaxies, respectively, in the four redshift bins. The contours give relative numbers of galaxies per area on the plot, for 2-armed galaxies (cyan contours) and 3-armed galaxies (black contours). In Figure 4, we have placed vertical lines marking the 90% completeness limit using the strict cut-off of $I_E = 20.5$, plus the 50% completeness limit with the more relaxed cut-off of $I_E = 21$.

In Figure 4, we have color-coded the datapoints based on Sérsic index. In all four panels, there is a trend of Sérsic index with concentration: galaxies with larger concentrations have higher mean Sérsic indices. Only a small subset of the galaxies in our sample have Sérsic index greater than 3; most of these are 2-armed galaxies. Very few 3-armed galaxies have Sérsic indices greater than 2. The high mass, high concentration galaxies tend to have larger Sérsic indices (up to ~ 4 , typical of elliptical-like galaxies), while low concentration galaxies tend low Sérsic indices, around 1, as expected from flat disk galaxies. Even in the high redshift ranges we see some Sérsic index = 4 galaxies among the 2-armed galaxies.

In all four panels in Figure 4, for a given stellar mass the 3-armed galaxies tend to have smaller concentrations than the 2-armed galaxies. We show this same result in a different way in the left panel of Figure 5, where we bin the galaxies into mass bins with bin size $\Delta(\log M^*) = 0.2$, and compare the median concentrations for the 2-armed and 3-armed galaxies as a function of redshift for the first and second redshift ranges. For a given redshift and mass range, 2-armed galaxies tend to have larger concentrations than 3-armed galaxies. If Figure 4 and Figure 5 were made using a 2-armed vote threshold of ≥ 0.5 rather than ≥ 0.8 , this conclusion would not change.

We ran Kolmogorov-Smirnov (KS) and Anderson-Darling (AD) tests to search for significant differences in the concentrations of the galaxies. For the $0.2 < z \leq 0.4$ redshift range, we found significantly larger concentrations for the 2-armed galaxies than for the 3-armed galaxies in all the mass bins between $9.9 \leq \log(M^*/M_\odot) < 10.1$ and $10.9 \leq \log(M^*/M_\odot) < 11.1$ (KS/AD probabilities of the samples being drawn from the same parent sample are ≤ 0.002). Similar statistics are found when the selection criteria for 2-armed galaxies is relaxed to vote fraction ≥ 0.5 rather than ≥ 0.8 . For the $0.4 < z \leq 0.6$ range, for all the mass bins between $10.1 \leq \log(M^*/M_\odot) < 10.3$ and $11.1 \leq \log(M^*/M_\odot) < 11.3$ the KS/AD probabilities are ≤ 0.006 , with the 2-armed galaxies having larger concentrations. Similar tests for $0.6 < z \leq 0.8$ give significant differences between 2-armed and 3-armed galaxies in all mass bins between $10.5 \leq \log(M^*/M_\odot) < 10.7$ and $11.3 \leq \log(M^*/M_\odot) < 11.5$, with KS/AD probabilities ≤ 0.007 . For the highest redshift range,

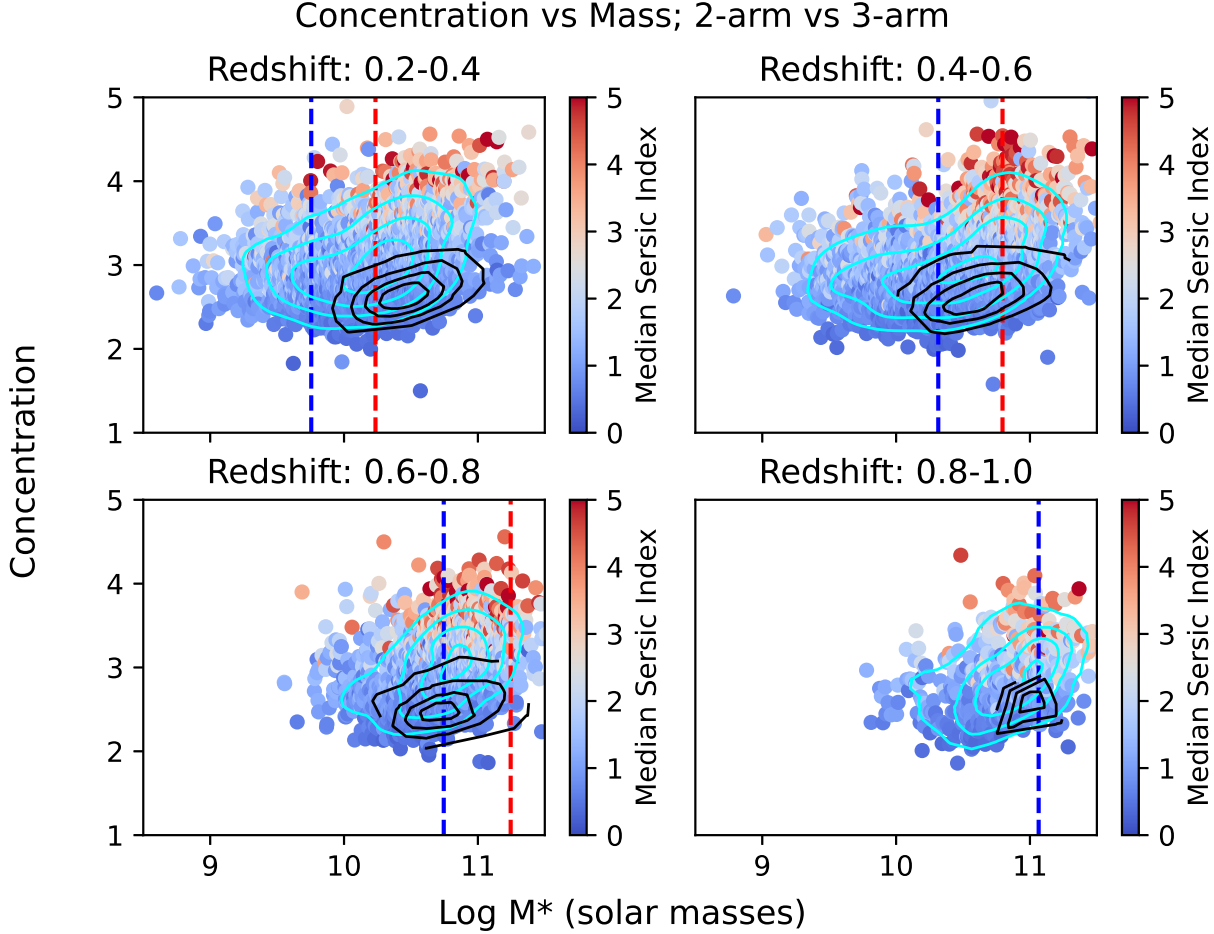


Figure 4. Concentration vs. $\log M^*$ for four redshift ranges, for galaxies in our samples of highly reliable 2-armed and 3-armed galaxies. The contours give relative numbers of galaxies per area on the plot, for 2-armed galaxies (cyan contours) and 3-armed galaxies (black contours). Concentration is defined as $C = 5 \log_{10} (r_{80}/r_{20})$ (Kent 1985; Conselice 2014), where r_{80} and r_{20} , respectively, are the radii containing 80% and 20% of the total Euclid visible light flux. The background color scale gives the median Sérsic index. The blue dashed vertical lines represent the 50% completeness limit assuming a magnitude limit of $I_E = 21$, while the red dashed lines are the 90% completeness limit assuming a limit of $I_E = 20.5$.

only the $11.1 \leq \log (M^*/M_\odot) < 11.3$ mass bin shows significant difference, with poorer but still significant KS/AD probabilities of 0.02.

The catalogued concentrations of the 2-armed galaxies in the $0.2 < z \leq 0.4$ range are larger than those of 2-armed galaxies in the $0.4 < z \leq 0.6$ range (left panel, Figure 5). In the mass bins between $9.9 < \log (M^*/M_\odot) \leq 10.1$ and $11.1 < \log (M^*/M_\odot) \leq 11.3$, this difference is significant, with KS/AD probabilities ≤ 0.003 , except in the highest and lowest mass bins, which have KS/AD probabilities ≤ 0.02 . This apparent different in concentration with z may be an artifact caused by redshift biases. Two different factors may contribute: poorer effective spatial resolution at higher redshifts, and shorter rest wavelengths at higher redshifts (i.e., a morphological K-correction). Numerous studies have shown that, if images of nearby spiral galaxies are smoothed to mimic the effect of higher redshifts, observed concentrations tend to decrease (Whitney et al. 2021; Thorp et al. 2021; Yu et al. 2023; Wang et al. 2024; Sazonova et al. 2025). Smoothing tends to increase r_{20} , therefore decreasing the measured concentration. The redshift bias in concentration has been quantified in these earlier studies in terms of the galaxy size (either effective radius or r_{90}) divided by either the FWHM of the point spread function, or the pixel size. For our sample galaxies, the median Kron radius (roughly r_{90} ; Graham & Driver 2005) is about $6'' - 7''$, and the median half-light radius is about $1''.1 - 1''.3$, with little variation between our two redshift bins. Given the pixel size and resolution of the Euclid images, published

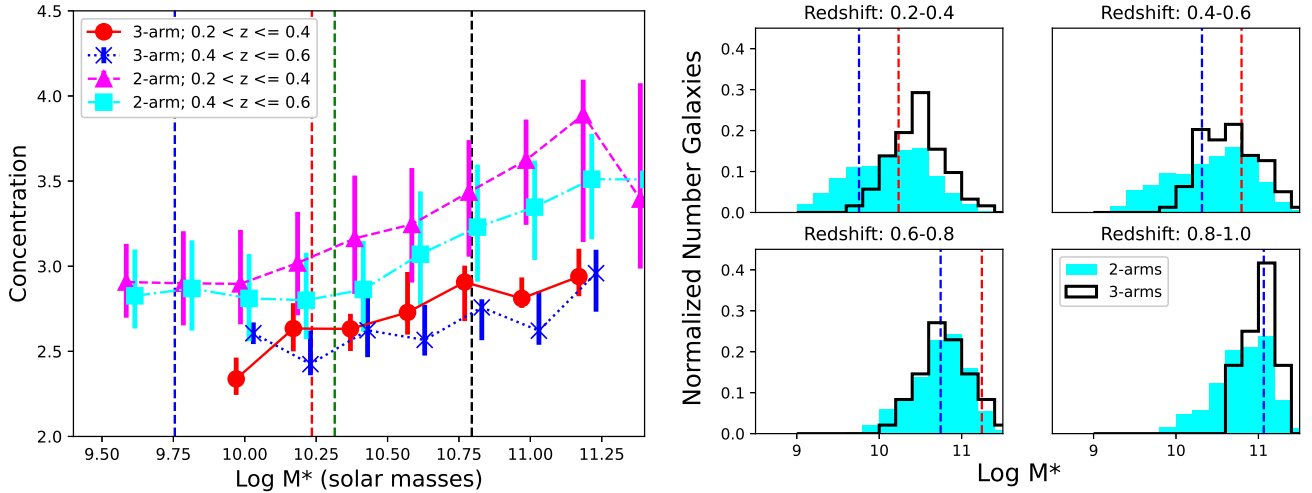


Figure 5. Left: After binning into stellar mass bins with bin size $\Delta(\log M^*) = 0.2$, this plot displays the median concentrations as a function of stellar mass for 2-armed galaxies in the $0.2 < z \leq 0.4$ range (cyan squares), 2-armed galaxies in the $0.4 < z \leq 0.6$ range (magenta triangles), 3-armed galaxies in the $0.2 < z \leq 0.4$ range (red circles), and 3-armed galaxies in the $0.4 < z \leq 0.6$ range (blue crosses). The errorbars display the range from the first to the third quartile. The datapoints have been slightly offset in the x direction to avoid overlap. The dark blue dashed vertical line represents the 50% completeness limit at $0.2 < z \leq 0.4$ assuming a magnitude limit of $I_E = 21$, while the red dashed line is the 90% completeness limit in the $0.2 < z \leq 0.4$ range assuming a limit of $I_E = 20.5$. The cyan (light blue) dashed vertical line represents the 50% completeness limit at $0.4 < z \leq 0.6$ assuming a magnitude limit of $I_E = 21$, while the black dashed line is the 90% completeness limit at $0.4 < z \leq 0.6$ assuming a limit of $I_E = 20.5$. Right: Histograms of the stellar masses for the 2-armed galaxies (filled cyan histograms) and the 3-armed galaxies (histograms outlined in black) in the four redshift ranges. Each histogram has been normalized so that the total area under the curve is equal to 1. The dark blue dashed vertical lines represent the 50% completeness limit in the plotted redshift range assuming a magnitude limit of $I_E = 21$, while the red dashed lines are the 90% completeness limit in the redshift range assuming a limit of $I_E = 20.5$.

correction tables (Wang et al. 2024; Sazonova et al. 2025) imply that the corrections to the measured concentrations due to redshift are small, ≤ 0.1 , and are not expected to vary too much with redshift in our redshift range. For 2-armed galaxies, we see an observed difference in concentration of about 0.2 between $z \sim 0.3$ and $z \sim 0.5$. This is larger than the expected effect due to resolution, indicating a possible residual difference in concentration. To test this in detail, for each 2-armed galaxy in the sample we applied the Sazonova et al. (2025) correction prescription to the concentration, and re-ran the KS/AD tests. We again obtained low KS/AD probabilities, indicating significant differences even after this correction.

This calculation, however, does not take into account possible changes in morphology with wavelength, which may also contribute to the observed redshift variations in concentration. At low redshifts, we observe longer rest wavelengths than at higher redshifts, and bulge stars contribute more at longer wavelengths. The change in concentration with redshift due to this effect has been quantified by Taylor-Mager et al. (2007), who measured concentrations of 199 nearby galaxies in several UV and optical filters. The Euclid I_E filter at $z = 0.3$ has a rest wavelength roughly equivalent to the optical V filter, while the rest wavelength observed by the Euclid filter at $z = 0.5$ approximately corresponds to the optical B filter. The median concentrations in the V and B filter for the Sa – Sc galaxies in the Taylor-Mager et al. (2007) sample are 2.87 and 2.71, respectively, giving a differential concentration of 0.13. When this offset of 0.13 plus the resolution correction is added to the observed Euclid concentrations of the galaxies in the $0.4 < z \leq 0.6$ redshift range, the concentrations agree well with galaxies at $0.2 < z \leq 0.4$ in the same mass range, and KS/AD probabilities show that we cannot rule out that the two sets of galaxies come from the same parent sample. The only mass bin for which we still see a significant difference in the concentrations is the $10.3 \leq (M^*/M_\odot) < 10.5$ bin. After both corrections were applied, the galaxies in the lower redshift range still have significantly higher concentrations (KS/AD probabilities < 0.001). In Section 5.3. we discuss these differences further. In contrast to the 2-armed

galaxies, KS/AD tests do not show significant differences in the concentrations of the 3-armed galaxies between these two redshift ranges.

In the two lower redshift ranges, the distribution of stellar masses for the 3-armed galaxies is shifted to higher masses compared to the 2-armed galaxies (Figure 4). In the $0.2 < z \leq 0.4$ redshift range, 3-armed galaxies tend to be both more massive and less concentrated than 2-armed galaxies. At $0.2 \leq z < 0.4$, the maxima for both samples are above the nominal 50% mass completeness limit, thus these offsets in mass are probably not caused by incompleteness. These results are shown more clearly in the right panel of Figure 5, where we provide histograms of the stellar masses of 2-armed vs. 3-armed galaxies for our four redshift bins. In the two lowest redshift ranges, the distribution of stellar masses for 2-armed galaxies is skewed to lower masses than that of 3-armed galaxies. KS/AD tests show that these differences are significant (KS/AD probabilities ≤ 0.001). In these two redshift ranges, there is a shortage of 3-armed galaxies below about $\log(M^*/M_\odot) = 10$, relative to 2-armed galaxies. This deficiency of low mass 3-armed galaxies does not appear to be caused by incompleteness, given that the completeness limits for 2-armed and 3-armed galaxies are similar. These trends do not change when the 2-arm vote fraction threshold is decreased to 0.5. We discuss possible explanations for the mass difference between 2-armed and 3-armed galaxies in Section 5.2. In the $0.6 < z \leq 0.8$ and $0.8 < z \leq 1.0$ redshift ranges, KS/AD tests do not show significant differences in the mass distributions of the two samples, perhaps because of incompleteness at the low mass end.

In the first two panels of Figure 4, there is a clear bend in the concentration-vs-stellar mass relation for 2-armed galaxies. Above about $\log(M^*/M_\odot) = 10.3$, a population of high concentration 2-armed galaxies exists. For 3-armed galaxies, higher mass galaxies tend to have larger concentrations, however, the relation appears linear; no bend is seen. Above $\log(M^*/M_\odot) = 10.3$, the low concentration galaxies in our sample are mostly 3-armed rather than 2-armed. In the $0.6 < z \leq 0.8$ and $0.8 < z \leq 1.0$ samples of 2-armed galaxies, there is still an apparent bend in the relation for 2-armed galaxies.

3.4. The Star-Forming Galaxy Main Sequence

The galaxy main sequence is a well-known correlation between \log SFR and $\log M^*$ for star-forming galaxies (Noeske et al. 2007; Salim et al. 2007). In Figure 6, we plot \log SFR vs. $\log M^*$ for our highly reliable 2-armed and 3-armed galaxies, dividing the galaxies into our four redshift ranges. We mark completeness limits by vertical lines. In making Figure 6, we excluded galaxies with $\text{SFR} < 10^{-2.5} M_\odot \text{ yr}^{-1}$ (i.e., $\log \text{sSFR} < -12$ for $M^* \geq 10^{9.5} M_\odot$), since sSFR at these low levels are very uncertain (Schiminovich et al. 2007; Salim et al. 2016). Galaxies with $\log \text{SFR} < -2.5$ constitute $< 3\%$ of the galaxies in the $0.2 < z \leq 0.4$ range. When Figure 6 is created using a 2-arm vote fraction threshold of 0.5 rather than 0.8, its appearance changes only slightly.

In Figure 6, in the $0.2 < z \leq 0.4$ range the distribution of SFRs peaks at higher SFRs for the 3-armed galaxies. However, the 3-armed galaxies also have higher stellar masses. In the lowest redshift range, the 2-armed and 3-armed galaxies make a single continuous sequence, with the distribution of 3-armed galaxies peaking at higher SFRs and higher stellar masses than the 2-armed galaxies. With increasing redshift, the bottom of the main sequence disappears because of incompleteness.

To compare the SFRs of the 2-armed and 3-armed galaxies more quantitatively, we binned the galaxies into $\Delta(\log M^*) = 0.2$ mass bins and ran KS/AD tests comparing the SFRs of the 2-armed and 3-armed galaxies at a given redshift and in a given mass bin. When comparing galaxies with similar stellar masses and redshifts, 2-armed and 3-armed galaxies have similar SFRs, except in a few mass ranges in the higher redshift bins, where the 3-armed galaxies have higher SFRs on average. In the $0.2 < z \leq 0.4$ range, we see no significant difference between 2-armed and 3-armed galaxies in any mass range. In the $0.4 < z \leq 0.6$ range, in two mass bins ($10.3 \leq \log(M^*/M_\odot) < 10.5$ and $10.7 \leq \log(M^*/M_\odot) < 10.9$), the 3-armed galaxies have significantly larger SFRs than the 2-armed galaxies (KS/AD probabilities ≤ 0.001 and ≤ 0.03 for the two bins, respectively). In the $0.6 < z \leq 0.8$ range, in only one mass bin ($11.1 \leq \log(M^*/M_\odot) < 11.3$) is there a marginally significant difference (KS/AD probabilities of 0.04/0.05), again with the 3-armed galaxies having higher SFR. No clear differences are seen in the highest redshift range.

In Figure 6, we overlay published main sequences (Speagle et al. 2014; Popesso et al. 2023; Euclid Collaboration: Enia et al. 2025) on the Euclid plots. In the lowest redshift range, the relation for our spirals agrees well with the earlier Euclid result (Euclid Collaboration: Enia et al. 2025), but lies slightly above other published main sequence relations (Speagle et al. 2014; Popesso et al. 2023), with SFRs enhanced by a factor of ~ 2 compared to their main sequence. Most of the 2-armed and 3-armed galaxies in our sample are close to the main sequence or above it, but in the middle redshift ranges, a few high mass 2-armed galaxies lie below the published main sequence. Although some

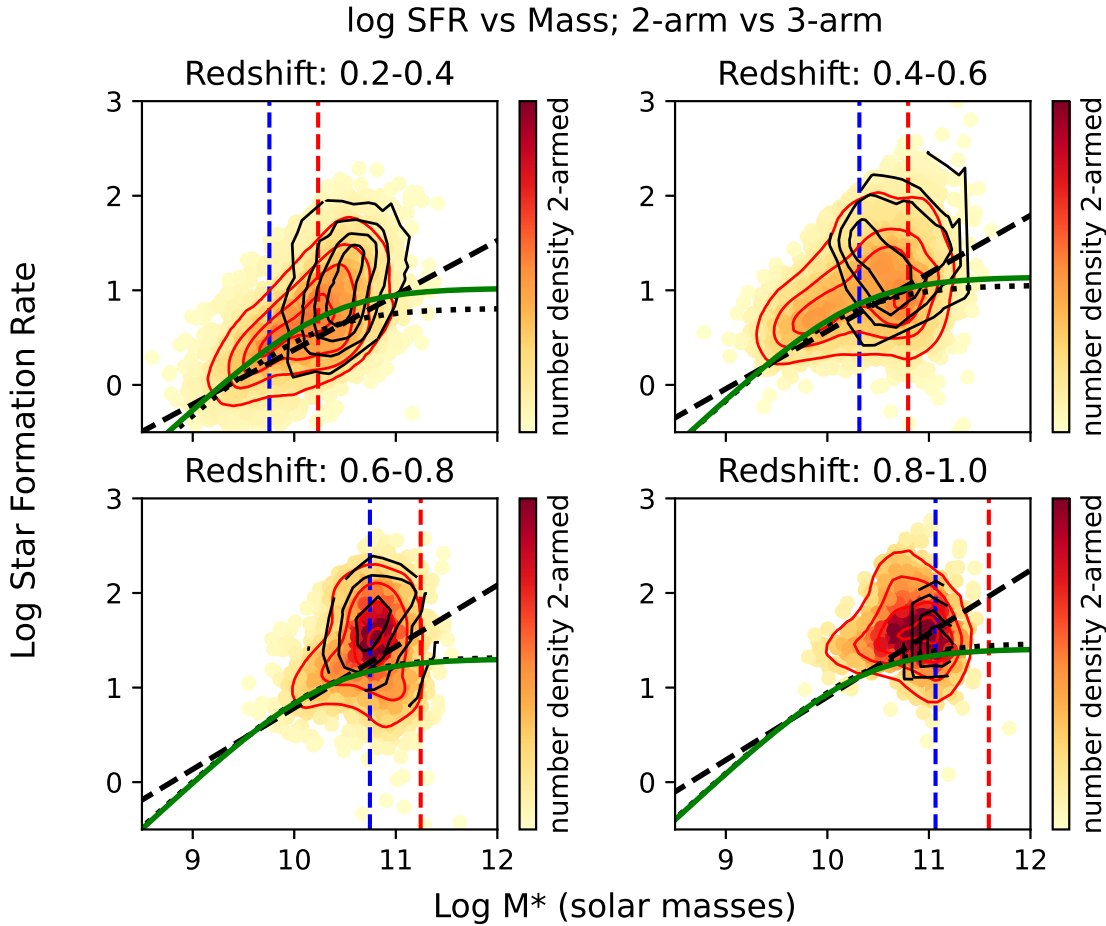


Figure 6. SFR (in solar masses per year) vs. $\log M^*$ for four redshift ranges, for galaxies in our highly reliable samples of 2-armed and 3-armed galaxies. The contours give the relative number density of 2-armed (red contours) and 3-armed galaxies (black contours) per area on the plot. The background color scale gives the relative number density of 2-armed galaxies on the plot, as shown in the color scales on the right. The blue dashed vertical lines represent the 50% completeness limit assuming a magnitude limit of $I_E = 21$, while the red dashed vertical line is the 90% completeness limit assuming a limit of $I_E = 20.5$. The star-formation main sequence from [Speagle et al. \(2014\)](#) is plotted as a black dashed line, while that of [Popesso et al. \(2023\)](#) is the dotted black curve. The solid green curve is the main sequence from [Euclid Collaboration: Enia et al. \(2025\)](#).

red spirals have been identified, they are relatively rare ([Masters et al. 2010](#)). Once star formation has dimmed, we cannot easily pick out spiral patterns.

To test whether SFR is a function of concentration at fixed stellar mass for the galaxies in our sample, we divided our 2-armed and 3-armed galaxies into two groups by concentration ($C \leq 3.2$ and $C > 3.2$), and then binned the galaxies by mass into bins with width $\log M^* = 0.3$. [Figure 7](#) plots the median concentration in each subset as a function of $\log M^*$. We then ran KS/AD tests in each M^* bin, comparing the sSFRs for high and low concentration galaxies for a given arm count. Since there are few high concentration 3-armed galaxies in our sample, for most mass bins we are only comparing 2-armed vs. 2-armed galaxies in the two concentration ranges. For only one bin did we find a significant difference: in the $10.7 \leq \log (M^*/M_\odot) < 11.0$ bin, the sSFRs for high concentration 2-armed galaxies are significantly lower than those of low concentration galaxies (KS/AD probabilities of 0.0013/0.0010, respectively). This suggests that at the high mass end of the main sequence, there may be some quenching of 2-armed spirals with bulge growth.

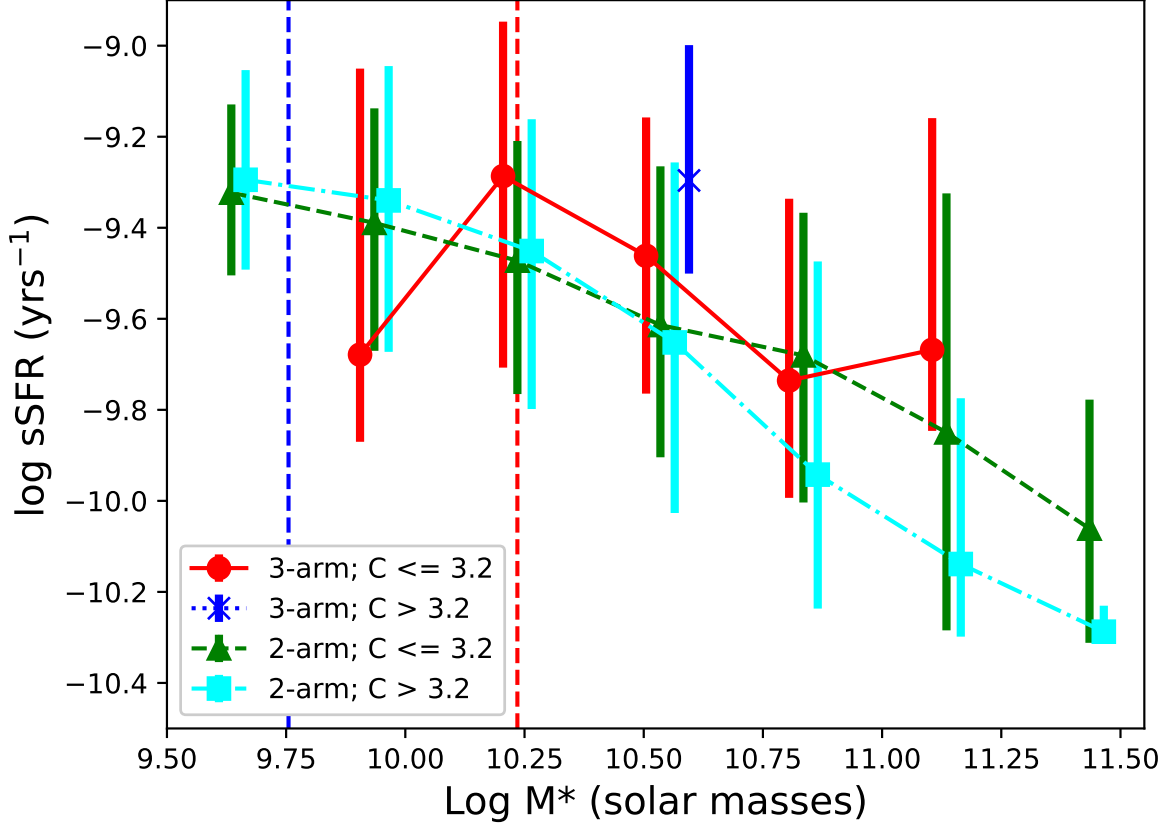


Figure 7. After binning into stellar mass bins with bin size $\Delta(\log M^*) = 0.3$ and dividing into two concentration bins, this plot displays the median sSFR as a function of stellar mass for 2-armed galaxies vs. 3-armed galaxies in the $0.2 < z \leq 0.4$ range. The errorbars display the range from the first to the third quartile. The datapoints have been slightly offset in the x direction to avoid overlap. The dark blue dashed vertical lines represent the 50% completeness limit at $0.2 < z \leq 0.4$ assuming a magnitude limit of $I_E = 21$, while the red dashed lines are the 90% completeness limit in the $0.2 < z \leq 0.4$ range assuming a limit of $I_E = 20.5$. This plot excludes datapoints for bins with two or less galaxies.

4. ONE-ARMED GALAXIES

In Figure 8, we compare our highly reliable samples of 1-armed and 2-armed galaxies. In the top row of Figure 8, we plot concentration vs. $\log M^*$ for $0.2 < z \leq 0.4$ (left panel) and $0.4 < z \leq 0.6$ (right panel). These plots show that 1-armed galaxies generally have lower stellar masses than 2-armed galaxies, however there is considerable scatter. For a given stellar mass, the concentrations and SFRs of 1-armed galaxies are similar to those of 2-armed galaxies. After binning the data into $\Delta(\log M^*) = 0.2$ mass bins, KS/AD tests show no significant differences in the concentrations of 1-armed and 2-armed galaxies with the same mass, except in the $10.5 \leq \log(M^*/M_\odot) < 10.7$ mass range at $0.2 < z \leq 0.4$, where the one armed galaxies have larger concentrations, a result that is marginally significant (KS/AD probabilities of 0.04/0.03, respectively). Also, in the $9.7 \leq \log(M^*/M_\odot) < 9.9$ mass bin for $0.4 < z \leq 0.6$, 2-armed galaxies have marginally larger concentrations (KS/AD probabilities of 0.01 and 0.02, respectively).

In the top panels of Figure 8, the datapoints shown are the values for the 1-armed galaxies after color-coding to the Sérsic index. The 1-armed galaxies tend to have low Sérsic indices, ~ 1 , typical of flattened disks, however, a handful of 1-armed galaxies with large concentrations also have large Sérsic indices.

In the bottom row of Figure 8, we plot \log SFR vs. $\log M^*$ for 1-armed vs. 2-armed galaxies at $0.2 < z \leq 0.4$ (left panel) and $0.4 < z \leq 0.6$ (right panel). In the lower redshift range, KS/AD tests show no significant difference between

the SFRs of 2-armed and 1-armed galaxies in the same mass range. In the $0.4 < z \leq 0.6$ range, the 1-armed galaxies have significantly larger SFRs than 2-armed galaxies of the same mass only for the $10.3 \leq (\log M^*/M_\odot) < 10.5$ and $10.7 \leq \log (M^*/M_\odot) < 10.9$ mass bins (KS/AD probabilities ≤ 0.001 and ≤ 0.003 , respectively).

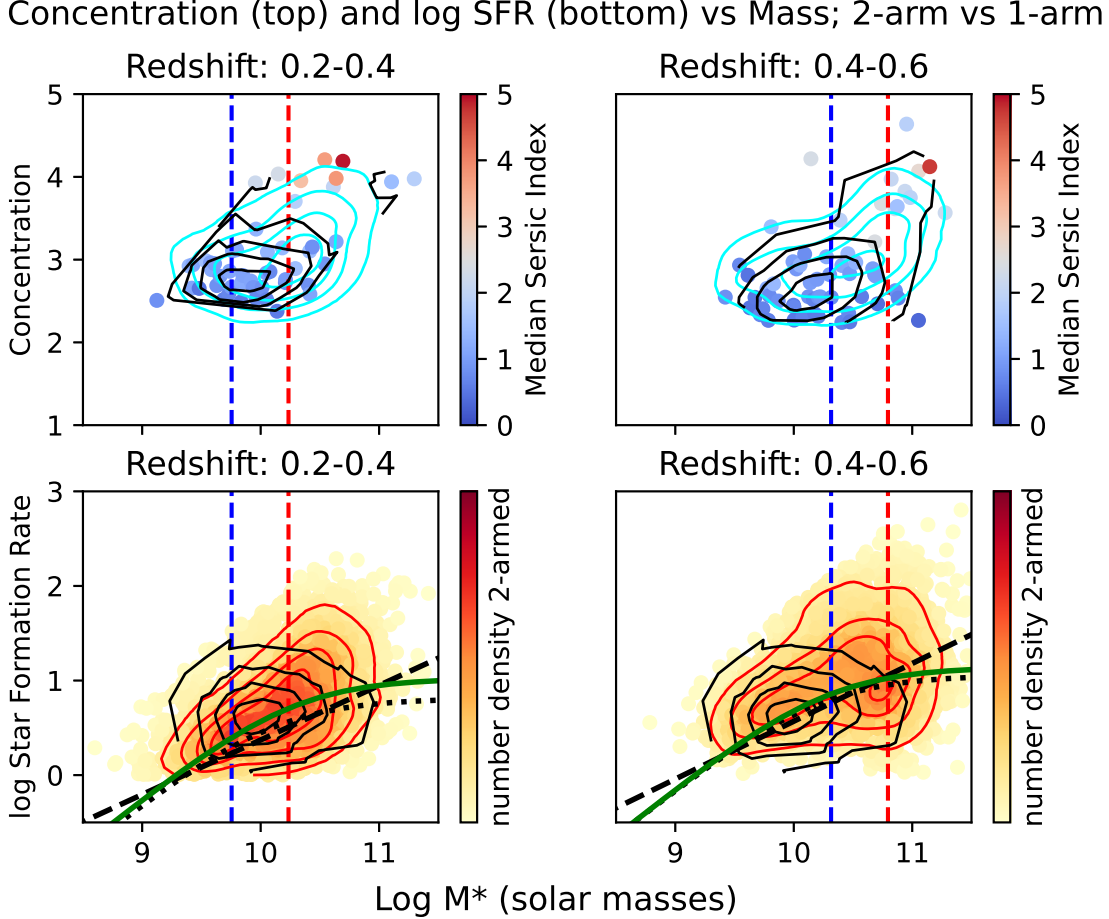


Figure 8. Top row: Concentration vs. $\log M^*$ for $0.2 < z \leq 0.4$ (left) and $0.4 < z \leq 0.6$ (right), for galaxies in our highly reliable samples of 2-armed and 1-armed galaxies. The contours give the relative number of galaxies per area on the plot for 2-armed (cyan contours) and 1-armed galaxies (black contours). The background color scale gives the Sérsic index of the 1-armed galaxies on the plot, as shown in the color scales on the right. Bottom row: Log SFR (in solar masses per year) vs. $\log M^*$ for $0.2 < z \leq 0.4$ (left) and $0.4 < z \leq 0.6$ (right). The contours give the relative number of galaxies per area on the plot for 2-armed (red contours) and 1-armed galaxies (black contours). The color scale displays the relative number density of 2-armed galaxies on the plot. In all four panels, the blue dashed vertical lines represent the 50% completeness limit assuming a magnitude limit of $I_E = 21$, while the red dashed vertical lines are the 90% completeness limit assuming a limit of $I_E = 20.5$. In panels in the bottom row, the star-formation main sequence from [Speagle et al. \(2014\)](#) is plotted as a black dashed line, while that of [Popesso et al. \(2023\)](#) is the dotted black curve. The solid green curve is the main sequence from [Euclid Collaboration: Enia et al. \(2025\)](#).

5. DISCUSSION

5.1. Arm Counts vs. Concentration, M^* , and SFR

Using data from the Euclid catalogs, we find 2-armed galaxies have larger concentrations than 3-armed galaxies for a given stellar mass. This result has been seen before in more nearby galaxies ([Elmegreen & Elmegreen 1982](#); [Bittner et al. 2017](#); [Yu & Ho 2020](#); [Smith et al. 2024](#)). With Euclid, we have extended this trend out to a redshift of 1. We also find that 2-armed galaxies tend to have larger Sérsic indices than 3-armed galaxies. This result is not

surprising since Sérsic index is well-correlated with concentration (Euclid Collaboration: Quilley et al. 2025). This result is consistent with expectations of spiral density wave theory, which suggests that a large bulge may stabilize a spiral density wave, allowing a 2-armed spiral pattern to persist (Lin & Bertin 1985; Bertin et al. 1989a,b; Saha & Elmegreen 2016). Two-armed spirals are also created in simulations of disk instabilities in isolated galaxies, if the disk mass is large compared to the halo and the bulge is large enough (Grand et al. 2013; D’Onghia 2015; Michikoshi & Kokubo 2018; Patsis & Okalidis 2025). Galaxies with large bulges tend to have declining rotation curves, which in turn produces a large shear rate, which favors 2-armed morphologies (Grand et al. 2013; D’Onghia 2015; Michikoshi & Kokubo 2018; Patsis & Okalidis 2025). Tidal interactions with low mass companions can also generate 2-armed patterns (Byrd & Howard 1992), even in very low density environments (Quinn et al. 2025). The presence of a bulge may allow a 2-armed pattern to last longer, whether the spiral structure is triggered by an interaction or by a random fluctuation in the disk. Buta et al. (2015) distinguish between normal grand design galaxies and a subset of systems they call ‘extreme spirals’. They define ‘extreme spirals’ as 2-armed galaxies with large amplitude arms and very open spirals. They suggest that many of these could be tidal spirals. This concept of two distinctly different types of 2-armed spirals deserves more exploration in future studies.

In the lowest redshift range studied in this survey, $0.2 \leq z < 0.4$, we see a difference in the stellar masses of 2-armed and 3-armed galaxies, with 3-armed galaxies being more massive on average. This is consistent with SDSS studies of more nearby galaxies (Smith et al. 2024). Why such a mass dependence exists is discussed below in Section 5.2. Because of sample incompleteness we cannot make clear conclusions about mass differences between 2-armed and 3-armed galaxies at $z > 0.4$.

At $0.2 < z \leq 0.4$, the 3-armed galaxies tend to have higher SFRs than the 2-armed galaxies, but for a given stellar mass 2-armed and 3-armed galaxies have similar SFRs. This result is not surprising given the well-known main sequence correlation between SFR and stellar mass for star-forming galaxies (Noeske et al. 2007; Salim et al. 2007) and the tendency of 3-armed galaxies to have larger stellar masses than 2-armed galaxies. This result is consistent with earlier studies at lower redshifts. Using Galaxy Zoo 2 arm counts for SDSS galaxies, Hart et al. (2017a) and Hart et al. (2017b) found similar sSFRs for 2-armed and 3-armed galaxies, for stellar-mass-matched samples. Hart et al. (2017a) conclude that their results support a scenario in which spiral arms mark the distribution of star-forming gas in galaxies, but are not directly responsible for star formation triggering (e.g., Elmegreen 2002). Willett et al. (2015) also found that the slope and dispersion of the galaxy main sequence for SDSS galaxies is independent of arm count. In addition, Elmegreen & Elmegreen (1986) found no significant variations in the SFR per area in the disks of spiral galaxies as a function of arm class. Smith et al. (2024) found no significant difference between the sSFRs of grand design and multi-armed galaxies, when comparing galaxies with similar stellar masses and concentrations. However, grand design galaxies tend to have larger concentrations, and galaxies with larger concentrations tend to have lower sSFR. Similarly, Smith et al. (2022) found a weak correlation between the $m=3$ Fourier amplitude of spiral galaxies and the sSFR, but this disappeared when comparing galaxies with similar M^* and concentration.

In the higher redshift ranges, in a few mass ranges near the top of the main sequence the 3-armed galaxies have enhanced SFRs compared to 2-armed galaxies of the same stellar mass. This result needs to be confirmed with larger more complete samples and more reliable photometric redshifts. If confirmed, one possible explanation might be that gas inflow into the galactic center has triggered a central starburst in the 3-armed galaxies, which may eventually lead to a more massive bulge. This supports the idea that 3-armed morphologies are favored in turbulent gas-rich galaxies (Bland-Hawthorn et al. 2024; Espejo Salcedo et al. 2025), and suggests that disk gas fraction may be a factor in the evolution of spiral patterns in galaxies. Followup work with larger samples is needed to fully explore these issues.

Euclid Collaboration: Quilley et al. (2025) investigated the Sérsic indices of 1,312,068 Euclid Q1 galaxies with $I_E < 23$. They identify a large population of Sérsic index ~ 4 early-type galaxies below the main sequence between $10 \leq \log (M^*/M_\odot) \leq 11$. Along the main sequence, they find mostly Sérsic index ~ 1 up to about $\log (M^*/M_\odot) = 10.5$, above which the Sérsic index increases to a median of ~ 2 by $\log (M^*/M_\odot) = 11$. In this regime (high mass main sequence galaxies), Euclid Collaboration: Quilley et al. (2025) detect a large dispersion in the Sérsic index of the galaxies, suggesting that morphologies change while the galaxies are still star-forming. This is consistent with earlier statistical studies of galaxy populations over time which find that star formation quenching is correlated with bulge growth (van Dokkum et al. 2010; Papovich et al. 2015). However, whether quenching happens before, after, or during morphological change may depend upon environment (Euclid Collaboration: Gentile et al. 2025). Our data suggest that, at the beginning of this quenching process, galaxies may be low concentration multi-armed galaxies near the top of the main sequence. Then, after a merger or other bulge-building process, the concentration and Sérsic

index increases, and the galaxy goes through a phase where a 2-armed morphology is favored but the galaxy is still star-forming. In the final stage, the galaxy is completely quenched and has an early-type morphology.

We also compare the concentrations, stellar masses, and SFRs of 1-armed galaxies with 2-armed galaxies. Only about 1% of the spirals in our sample are classified as 1-armed. The 1-armed galaxies tend to have lower stellar masses than 2-armed galaxies, but with some scatter. The concentrations and SFRs of the 1-armed galaxies are similar to those of 2-armed galaxies with the same stellar mass. Simulations suggest that leading 1-armed spiral arms can be produced by retrograde interactions with a companion of similar mass (Thomasson et al. 1989; Howard et al. 1993). This would tend to bias 1-armed galaxies towards lower stellar masses than galaxies with two spiral arms, since grand design patterns can be produced by interactions with lower mass companions (e.g., Byrd & Howard 1992). For an SDSS sample of galaxies, Casteels et al. (2013) found that galaxies identified as 1-armed in Galaxy Zoo 2 were more likely to have close companions than a control sample, supporting the hypothesis that these are predominantly produced by tidal interactions. Our observation that 1-armed galaxies have similar concentrations and SFRs to 2-armed galaxies also supports the idea that $m=1$ structures are not a function of internal structural parameters, but instead are linked to tidal interactions. Followup study is needed of the 1-armed galaxies in this Euclid sample to confirm their morphologies, investigate their environments, and search for possible companions.

5.2. The Bend in the C vs. $\log M^*$ Relation

We see a bend in the concentration-vs-mass relation for 2-armed galaxies. In our lowest redshift bin, the bend occurs at about $\log (M^*/M_\odot) = 10.3$. In contrast, for 3-armed systems the concentration-mass relation is approximately linear, without a bend. At $\log (M^*/M_\odot) > 10.5$, we see a dichotomy among our spirals: low concentration galaxies have 3 arms, while high concentration galaxies have 2 arms. Such a bend has been seen before at lower redshifts by Luo et al. (2020) for disk galaxies in general, and for grand design galaxies by Smith et al. (2024). Luo et al. (2020) suggest that the bend in the C - $\log M^*$ relation of spirals is caused by the development of classical bulges in galaxies with higher overall stellar masses. Mergers between galaxies can build up the bulge of a spiral, potentially creating a classical bulge (Hopkins et al. 2010; Sachdeva et al. 2015, 2017) and therefore increasing the concentration. Secular processes such as bar-driven gas inflow followed by central star formation may also help to grow a bulge (Kormendy & Kennicutt 2004; Athanassoula 2005; Sellwood 2014). As discussed above, simulations suggest that a classical bulge is more able to maintain a grand design spiral pattern (Saha & Elmegreen 2016).

Perhaps not coincidentally, the bend in the C - $\log M^*$ relation lies close to the stellar mass at which the stellar-to-halo-mass function for galaxies in the local Universe reaches a maximum (Behroozi et al. 2010; Girelli et al. 2020). Galaxies with stellar masses higher or lower than about $\log (M^*/M_\odot) = 10.5$ show larger proportions of dark matter relative to stars. According to simulations, above this mass threshold the dominant method of galaxy growth is mergers, while below this threshold galaxy growth is dominated by gas accretion and star formation (Bouché et al. 2010). Above this threshold mass, star formation may be inhibited by virial shock heating of gas falling into a massive halo (Birnboim & Dekel 2003; Kereš et al. 2005; Dekel & Birnboim 2006; Cattaneo et al. 2006) and/or AGN feedback (Croton et al. 2006; Somerville et al. 2008). Below this mass threshold, baryons are selectively evicted from the galaxy by stellar winds (Dekel & Woo 2003), producing a correlation between M^*/M_{halo} and total mass.

In Figure 9, we provide a schematic diagram of concentration vs. $\log M^*$ for spiral galaxies, and indicate approximately the zones in which each of the three arm classes of galaxies are expected to dominate. Because of how our samples were selected, flocculent galaxies are largely omitted from our study. Earlier studies found that flocculent galaxies tend to be low mass, compared to grand design and multi-armed galaxies (Bittner et al. 2017). They also tend to have late Hubble types (Elmegreen et al. 2011; Ann & Lee 2013), and therefore low concentrations. In a plot of C vs. $\log M^*$, flocculent galaxies are therefore expected to lie in the lower left corner.

Moving horizontally in Figure 9 from the lower left towards larger masses while keeping the concentration fixed, M^*/M_{halo} would tend to increase, according to the stellar-mass-halo-mass function (Girelli et al. 2020), and therefore the ratio of disk mass to halo mass M_{disk}/M_{halo} would increase. Presumably this is the evolutionary path for a low mass, low concentration galaxy that accretes gas and forms disk stars. According to numerical simulations, a larger M_{disk}/M_{halo} favors multi-armed morphologies rather than flocculent patterns (D’Onghia et al. 2013; Fujii et al. 2018). This is consistent with our observation that 3-armed systems (i.e., multi-armed galaxies) tend to be massive but have low concentrations. This may be the reason that multi-armed galaxies tend to have high stellar masses; galaxies with lower stellar masses will have proportionally larger dark matter haloes, which favor flocculent rather than multi-armed morphologies.

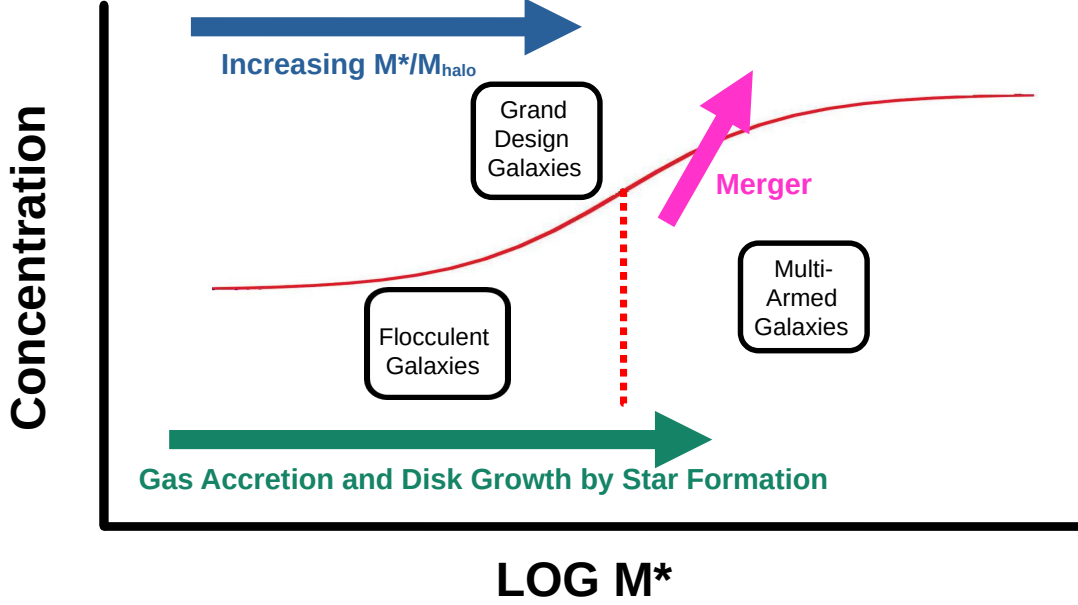


Figure 9. A schematic diagram of the concentration vs. $\log M^*$ plane for spiral galaxies. Tentative zones of importance for 2-armed (grand design), multi-armed, and flocculent galaxies are delineated by the curving red line and the dotted vertical line. Two-armed galaxies tend to have large concentrations with a range of masses, but lower concentrations at lower masses. Multi-armed galaxies tend to have low concentrations and high stellar masses, while flocculent galaxies are thought to have low stellar masses and low concentrations. As illustrated by the blue arrow pointing to the right, the ratio of stellar mass to halo mass M^*/M_{halo} tends to increase with increasing stellar mass, up to a maximum at about $\log (M^*/M_{\odot}) = 10.5$ (Girelli et al. 2020) (dotted red vertical line). On the left side of the plot, growth in the stellar mass of a galaxy is thought to be caused primarily by gas accretion followed by disk star formation, as shown by the green arrow. The magenta diagonal arrow represents the expected direction of evolution due to a merger, which is expected to increase the size of the bulge and therefore the concentration, and also increase the stellar mass.

Moving vertically upwards from the lower right in Figure 9 towards a larger concentration and larger bulge at a fixed stellar mass and fixed halo mass would favor 2-armed patterns over a multi-armed morphology. This holds for both spirals induced by disk instabilities and swing amplification (D’Onghia 2015; Michikoshi & Kokubo 2018) and long-lived spiral density waves (Saha & Elmegreen 2016). In a merger, both the bulge and the overall stellar mass of the galaxy will grow, causing the system to travel in an diagonal path upwards and to the right in Figure 9. Since bulge mass is correlated with black hole mass (Ferrarese & Merritt 2000; King 2003), and because the probability of radio-loud AGN activity increases as the mass of a black hole increases (Metcalf & Magliocchetti 2006; Garofalo et al. 2020), AGN quenching is more likely in galaxies with larger bulges. Alternatively, a growing bulge may quench star formation via ‘morphological quenching’ (Martig et al. 2009), a process in which a massive bulge stabilizes a gaseous disk against gravitational collapse, leading to a lower SFR. After a galaxy is quenched, the stellar mass only grows via mergers, thus galaxies tend to move diagonally upwards in Figure 9 after quenching. This scenario of gas accretion, star formation, feedback, quenching, and mergers may be responsible for the bend in the concentration-mass relation and the Σ_1 -mass relation (Luo et al. 2020; Barro et al. 2017; Gao et al. 2022; Cattaneo et al. 2025).

We suggest that, once a disk galaxy has passed the threshold of $\log (M^*/M_{\odot}) = 10.5$, it has two possible future evolutionary paths. If it does not undergo mergers or otherwise fatten its bulge, it will retain its low concentration, and will tend to have 3 or more arms. If it undergoes one or more mergers or grows its bulge by another process, then it becomes a 2-armed spiral, or an elliptical or S0 galaxy. If the galaxy exceeds this mass threshold and grows a sufficiently large bulge, star formation may start to slow down. We see evidence for this in Figure 7, where large-concentration 2-armed spirals in the $10.7 \leq \log (M^*/M_{\odot}) < 11.0$ mass range have significantly lower sSFR than low-concentration 2-armed spirals in the same mass bin. At lower masses, we do not see differences in sSFR between low and high concentration 2-armed galaxies at fixed mass. This supports the idea that bulge growth aids quenching in spirals, but this quenching only becomes important at high stellar masses, above the bend in the C vs $\log M^*$ plot. At masses

below the $\log(M^*/M_\odot) = 10.5$ threshold, most spiral galaxies tend to lie on the same main sequence, independent of the number of spiral arms. This result is consistent with SDSS studies, that showed that most red spiral galaxies are massive; few are found below our threshold mass (Masters et al. 2010; Fraser-McKelvie et al. 2018). Although low mass galaxies below the main sequence tend to have larger Sérsic indices than main sequence galaxies (Wuyts et al. 2011), implying larger concentrations, they generally do not have prominent spiral patterns. In a study of low mass red spirals, Fraser-McKelvie et al. (2018) found that they were only located in clusters, suggesting that they are the products of quenching caused by ram pressure stripping in dense environments. In less extreme environments, galaxies will retain their gas and therefore their spiral pattern, and will continue to evolve up the main sequence, only quenching near the high mass end.

One possible test of these ideas is to determine the M^*/M_{halo} function for 2-armed and 3-armed galaxies independently. One might expect lower M^*/M_{halo} ratios in galaxies with larger concentrations if they suffered more mergers over their lifetimes, since mergers add dark matter as well as additional stars. Thus 2-armed galaxies might tend to have lower M^*/M_{halo} ratios on average than 3-armed galaxies, for the same stellar mass. Conversely, if stellar mass growth in 3-armed/multi-armed galaxies has been dominated by gas accretion followed by star formation, they would be expected to have larger M^*/M_{halo} ratios.

At low masses, whether a galaxy is 2-armed or flocculent may depend upon the central mass of the galaxy. If a galaxy starts in the lower left of Figure 9 as a flocculent disk galaxy, and then builds a bulge or otherwise increases its central mass, it would tend to move upwards in the plot, into the regime where 2-armed morphologies are favored. Whether a spiral galaxy has two or more arms may depend in part upon the mass in the central core, whether this mass is in stars or dark matter. For a given disk mass, galaxies with high density cores are more likely to be 2-armed, while galaxies with lower density cores are more likely to be flocculent or multi-armed. How the dark matter is distributed in spiral galaxies is still uncertain. It is sometimes assumed that baryons dominate the mass in the inner parts of spiral galaxies (e.g., van Albada et al. 1985). However, detailed studies of the rotation curves of nearby spirals indicate that the disks of moderate-mass spirals are sub-maximal (Martinsson et al. 2013; Lelli et al. 2016; Starkman et al. 2018), meaning that dark matter dominates the mass even in the cores. In higher mass spirals, however, the dark matter contribution in the core appears to become less important, and the disks are near-maximal (Martinsson et al. 2013; Lelli et al. 2016; Starkman et al. 2018). Although the spatial distribution of dark matter in the inner parts of spiral galaxies is quite uncertain (Ponomareva et al. 2026), the distribution of dark matter in the inner regions of low mass spirals may trace that of the baryons (Lelli et al. 2016). If this is the case, this suggests that low mass spirals with larger stellar bulges may have proportionally larger dark matter concentrations in their cores, favoring 2-armed morphologies. This contribution from dark matter to the central mass may move the boundary between 2-armed and flocculent galaxies downwards in Figure 9, causing low mass 2-armed galaxies to have relatively low concentrations in optical images. An increasing M_{disk}/M_{halo} ratio with increasing stellar mass may be responsible for the bend in the concentration vs. $\log M^*$ relation, and the threshold at $\log(M^*/M_\odot) = 10.5$ may correspond to the point at which the disk becomes maximal. We suggest that two parameters control the arm count in spiral galaxies: the relative mass of the disk and halo, and the central mass density. If the mass distribution is centrally-concentrated, it would favor a dominant 2-armed structure. In contrast, galaxies with lower central mass densities will be either multi-armed or flocculent, depending upon the relative disk vs. halo mass.

To test these ideas, it is important to properly map the C-log M^* plot shown in Figure 9 and better determine the boundaries between the different arm classes. This requires more complete samples of spirals that also include flocculent galaxies. It also requires better methods for counting the numbers of arms in galaxies (see Section 5.4). It would also be valuable to use rotation curves to measure the dynamical mass distributions in galaxies of different arm classes and different stellar masses. Do the rotation curves of 2-armed and 3-armed galaxies differ? Do 2-armed galaxies have larger shear than 3-armed galaxies? For the same stellar mass, are 3-armed galaxies more likely to have maximal disks than 2-armed galaxies? The answers to these questions will shed light on the nature of spiral arms in galaxies.

5.3. Bulge Growth?

When comparing 2-armed galaxies in our two lowest redshift ranges, $0.2 < z \leq 0.4$ and $0.4 < z \leq 0.6$, the galaxies in the lower redshift range have higher observed concentrations for the same mass. Most of this difference can be accounted for by morphological K-corrections plus a bias due to lower effective resolution at larger distances. We cannot, however, rule out bulge growth as a contributing factor.

According to IllustrisTNG cosmological simulations, bulges have grown significantly between $z \sim 2$ and $z = 0$ (Tacchella et al. 2019). The observational evidence for recent bulge growth in spiral galaxies, however, is mixed. An analysis of stellar populations in nearby spirals using Calar Alto Legacy Integral Field Area (CALIFA) data suggests that bulges formed early and did not evolve much over time (Méndez-Abreu et al. 2021). This is consistent with models in which bulges form in the early Universe, via disk instabilities, clump migration, and other processes in gas-rich disks (Bournaud et al. 2011; Dekel et al. 2009; Dekel & Burkert 2014; Zolotov et al. 2015). On the other hand, bulge-disk decompositions led Sachdeva et al. (2017) to conclude that bulge masses have increased by a factor of two since $z \sim 1$, while Tasca et al. (2014) concluded that the luminosities of bulges have grown by 30% since $z \sim 0.8$.

Several properties of galaxies that might affect the C-log M^* relation are known to vary with redshift. These include the fraction of galaxies with high Sérsic index radial light profiles (Bell et al. 2012), the SFR-vs- M^* relation (Speagle et al. 2014; Popesso et al. 2023), the size- M^* relation (van der Wel et al. 2014), and the stellar-mass-to-halo-mass function (Girelli et al. 2020). Future studies of the C-log M^* relations for different arm classes are needed using the full Euclid sample, better spiral classification methods, improved photometric redshifts, Euclid-specific redshift bias corrections, and detailed bulge/disk decompositions, to better address the question of bulge growth over time.

5.4. 2-Armed vs. Grand Design, 3-Armed vs. Multi-Armed: Comparison to Previous Studies

The ratio of the number of 2-armed galaxies to the number of 3-armed galaxies in our Euclid Zoobot study and in the Hart et al. (2016) Galaxy Zoo 2 study are similar to each other, but starkly different from earlier by-eye classifications by experts of the ratio of grand design to multi-armed galaxies. Some statistics from earlier studies are summarized in Table 2, along with details about the sample selection for each study. Elmegreen & Elmegreen (1987) used photographic images from the Palomar Observatory Sky Survey (POSS) and high resolution atlas photographs to determine arm classes for galaxies selected from the Second Reference Catalogue of Bright Galaxies (RC2; de Vaucouleurs et al. 1976). The Ann & Lee (2013) study used SDSS images for a volume-limited, absolute-magnitude-limited sample of galaxies. Buta et al. (2015) classified a distance-limited, blue magnitude-limited set of 1114 spiral galaxies into arm classes using Spitzer 3.6 μm images. Wei et al. (2024) determined arm classes for 5093 galaxies selected from a list of blue spirals published by Masters et al. (2010). The statistics in Table 2 are provided in two forms: first, by giving percentages in all three arm classes (grand design, multi-armed, and flocculent), and second, by omitting the flocculent galaxies and simply listing the ratio of grand design to multi-armed galaxies.

Table 2 shows considerable variations between these published studies. Part of this variation is due to sample selection. The masses of the galaxies is an important factor, since galaxies with different arm classes tend to have different masses. For example, the Buta et al. (2015) sample is distance-limited, so is more biased towards lower mass galaxies than SDSS-selected samples, and thus contains a larger proportion of flocculent galaxies. Another factor that probably contributes to the differences in Table 2 is the specific criteria used by the researchers to classify the galaxies. For example, Wei et al. (2024) categorize only 3% of their galaxies as grand design, the smallest fraction of grand design galaxies in Table 2. They use a very strict definition of grand design: “two long and continuous arms with strong symmetry” and “devoid of branching along the arms”. They state that with the improved resolution and sensitivity of the SDSS vs. earlier studies, they can detect bifurcations and discontinuities not previously seen, causing galaxies to be classified as multi-armed rather than grand design. Furthermore, they state that when a galaxy has only two arms in their inner region which “spread out” in the outer disk, they classify it as “multi-armed”. They note that more than half of the galaxies that they place in their “multi-armed” category have only two arms in their interiors. The Wei et al. (2024) selection criteria for grand design galaxies may favor galaxies that have recently suffered strong tidal interactions, i.e., the Buta et al. (2015) ‘extreme spirals’. These may be a small subset of all 2-armed galaxies.

In Table 2 we also list the percentage of galaxies classified as 2-armed in Hart et al. (2016) and in our Euclid study, compared to the sum of the percentages identified as 3-armed, 4-armed, and 5+-armed (collectively assumed to be multi-armed galaxies). We also provide the percentages of ‘can’t-tell’ spirals (possibly flocculent galaxies). Our Euclid percentages agree well with the Hart et al. (2016) GZ2 SDSS fractions. However, the fraction of galaxies placed in the flocculent arm class by experts are two to three times higher than the proportion of galaxies classified by the GZ2 volunteers/Euclid Zoobot as can’t-tell. The most likely explanation for this is that many flocculent galaxies are omitted from the spiral category by the GZ viewers/Zoobot.

Independent of the flocculent/cant-tell galaxies, the ratio of 2-armed/3+4+5+-armed galaxies in the SDSS GZ2 study and the Euclid Zoobot database is at least four times larger than the ratio of grand design/multi-armed galaxies in the earlier studies. Clearly, a classification as 2-armed by GZ2/Zoobot is not identical to a classification as grand

design by an expert. One reason for this difference is that many galaxies have two arms in their inner disks, which branch into multiple arms further out in the disk. In a careful by-eye classification by experts, this branching may be noticed, and the galaxy placed in the multi-armed group. In contrast, a volunteer GZ2 participant may take a cursory look and notice the two arms in the inner regions, and ignore branching further out in the galaxy. Perhaps the GZ2/Zoobot classifications are more heavily weighted towards the inner disks of the galaxies, while expert classifiers may consider the overall arm structure. The statistics in Table 2 strongly suggest that some of the galaxies selected as 2-armed by our initial selection criteria would be classified as multi-armed by experts.

In our Euclid study, our ‘highly reliable’ selection criteria more cleanly separates 2-armed galaxies from multi-armed galaxies compared to our original initial sample selection. The fact that these ‘highly reliable’ subsets of galaxies occupy different locations in concentration-log M^* plots demonstrates conclusively that they do not come from the same parent sample, but have fundamentally different structural and physical properties. However, the additional filtering used to construct these highly reliable subsets excludes a large number of galaxies with more uncertain arm counts, making determining the percentage of spirals in different arm classes very uncertain.

Few galaxies are truly completely 2-armed or completely 3-armed (or completely four-armed), but instead there is a continuum of morphologies, with branches and spurs being common. Our highly reliable 2-armed sample is presumably more weighted towards galaxies in which a 2-armed structure dominates, compared to the 3-armed sample. However, spiral arm structure is more complicated than the three simple categories of grand design, multi-armed, and flocculent. Likewise, the Galaxy Zoo 2/Zoobot arm counts, although informative, do not provide the complete story.

A more detailed arm identification system with twelve categories was introduced by Elmegreen & Elmegreen (1982). The additional information these 12 categories provide may be helpful in exploring questions about the origin and evolution of spiral patterns in galaxies. However, this 12-group method is more complicated and time-consuming to use than the simpler 3-class system, and would be difficult to implement in an automatic way for large samples of galaxies. Given the gigantic numbers of galaxies being observed by Euclid and soon the Nancy Grace Roman Telescope, there is a need for a simple-to-implement mathematical description of arm structure to cleanly separate galaxies into subsets based on arm properties. One possibility is a Fourier-type decomposition of images, a technique previously used for smaller numbers of galaxies (Grosbøl et al. 2004; Durbala et al. 2009; Elmegreen et al. 2011; Yu et al. 2018; Yu & Ho 2020). Determining Fourier components as a function of the radius of a galaxy would be helpful in identifying spiral arm branches and spurs, and could pick out galaxies with two arms in the interior and multiple arms at larger radii. An alternative classification method that may prove valuable in studying arm structure is fractal dimensions (Saha et al. 2025).

Employing a more detailed morphological classification scheme for spiral patterns in galaxies may lead to a better understanding of the various processes involved in creating and maintaining spiral patterns in galaxies. Perhaps there are distinctly different subclasses of 2-armed spirals, for example, those with transient $m=2$ patterns caused by disk instabilities, vs. long-lived 2-armed patterns with fixed pattern speeds, vs. tidally-triggered grand design spirals, vs. spirals associated with bars. A deeper look at subtle variations in the spiral structures and the physical properties of galaxies selected by different methods may lead to useful insights.

6. SUMMARY

The Euclid telescope Quick Data Release 1 (Euclid Collaboration: Mellier et al. 2025) has provided the Astronomical community with several catalogs of galaxy properties, containing photometric redshifts, stellar masses, concentrations, and SFRs (Euclid Collaboration: Tucci et al. 2025). For 380,111 galaxies, the Zoobot foundation model made estimates of the expected Galaxy Zoo 2 vote fraction for several morphological traits, including the number of spiral arms (Euclid Collaboration: Walmsley et al. 2025).

Filtering out galaxies with less reliable parameters, we placed each galaxy into an initial arm count class based on which class has the highest estimated vote fraction. We find that 65% of the $\log(M^*/M_\odot) \geq 10.6$ spirals with $0.175 \leq z < 0.275$ are 2-armed and 15% are 3-armed, if the ‘can’t count number of arms’ spirals are excluded. These statistics are consistent with the Hart et al. (2016) bias-corrected fractions for SDSS galaxies in the local Universe. Determining the fraction of spirals of different arm counts at higher redshifts, $z > 0.2$, is quite uncertain, due to sample incompleteness and redshift-dependent classification biases. Interestingly, however, Espejo Salcedo et al. (2025) classify 60% of JWST $z \sim 1$ $\log(M^*/M_\odot) \geq 10.0$ spirals as 2-armed, similar to the Euclid $z \sim 0.2$ Zoobot percentage. Although differences in classification metrics between the JWST study and the Zoobot may be substantial, as a first tentative attempt to investigate how spiral fractions vary in the $0.2 < z \leq 1$ window, based on these JWST observations we make

Table 2. Percentages of Grand Design, Multi-Armed, and Flocculent Galaxies

Reference	Grand Design	Multi-Armed	Flocculent	Ratio GD/MA	Images Used	Source/Catalog	Selection Criteria
Elmegreen & Elmegreen 1987	13%	42%	45%	0.31	POSS+Atlas	RC2	
Ann & Lee 2013	19%	38%	43%	0.5	SDSS		$z < 0.2$; $M_r < -16.1$
Buta et al. 2015	18%	32%	50%	0.56	Spitzer	S ⁴ G	$D < 40$ Mpc, $m_B < 15.5$
Wei et al. 2024	3%	59%	38%	0.05	SDSS		blue spirals

Reference	2-Armed	3+4+5+-Armed	Can't-tell	Ratio 2-Armed/3+4+5+-Armed	Images	Source/Catalog	Selection Criteria
Hart et al. 2016 ¹	55%	27%	17% ²	2.0	SDSS	GZ2	$\log M^* \geq 10.6$
This work ¹	54%	24%	22%	2.2	Euclid	Zoobot	$\log M^* \geq 10.6$

¹Excluding galaxies selected as 1-armed.

²Estimated from Figure 8 in Hart et al. (2016).

the simplifying assumption that the fraction of 2-armed spirals remains constant in this redshift range. Given this assumption, and making an approximate correction for redshift bias, we infer that the number of 3-armed galaxies increases slightly with redshift to $\sim 30\%$ at $z = 1$. This result is quite preliminary, and needs confirmation.

Filtering the samples further to only include ‘highly reliable’ 2-armed galaxies (vote fraction for 2-arms ≥ 0.8), ‘highly reliable’ 3-armed galaxies (vote fraction for 3-armed ≥ 0.5), and ‘highly reliable’ 1-armed galaxies (vote fraction of 1-armed ≥ 0.5), we identify 6284 2-armed, 262 3-armed galaxies, and 188 1-armed galaxies with $0.2 \leq z < 1$. The 1-armed galaxies tend to have lower masses than the 2-armed galaxies, but for a given stellar mass 1-armed galaxies have similar concentrations and SFRs as 2-armed galaxies. The 2-armed galaxies have larger concentrations, lower stellar masses, and lower SFRs, on average, than the 3-armed galaxies. The lower SFRs for 2-armed galaxies are a consequence of their lower stellar masses; for the same stellar mass, 2-armed and 3-armed galaxies have similar SFRs. These differences between 2-armed and 3-armed galaxies have been seen before in nearby galaxies (e.g., Smith et al. 2024). With Euclid we show that the trend with concentration continues out to $z = 1$, and the trend for mass and SFR to $z = 0.4$.

These results are consistent with theoretical models and simulations, which show that 2-armed galaxies are favored when the bulge is prominent (Lin & Bertin 1985; Bertin et al. 1989a,b; Grand et al. 2013; D’Onghia 2015; Saha & Elmegreen 2016; Michikoshi & Kokubo 2018; Patsis & Okalidis 2025), and multi-armed or flocculent morphologies appear in models with small or no bulge (D’Onghia et al. 2013; Fujii et al. 2018). We surmise that the lack of low mass 3-armed galaxies in our sample is a consequence of the known trend of smaller M^*/M_{halo} ratios in lower mass galaxies (Behroozi et al. 2010; Girelli et al. 2020). According to simulations, galaxies with large M^*/M_{halo} but small bulges tend to be multi-armed, but galaxies with small M^*/M_{halo} and similarly small bulges will be flocculent (D’Onghia et al. 2013; Fujii et al. 2018). Since our sample lacks flocculent galaxies, the low C, low M^* regime is only sparsely populated in our study. Followup studies are needed to better quantify where flocculent galaxies are located in C-log M^* space.

We see a bend in the concentration-log M^* relation for 2-armed galaxies at $M^* \approx 10^{10.3} M_\odot$. High mass 2-armed galaxies show significantly larger concentrations than their lower mass counterparts. In contrast, 3-armed galaxies reveal a linear correlation between concentration and log M^* , without a bend. We explain the bend in the C-log M^* relation for 2-armed galaxies as being the result of several factors: 1) an increasing M^*/M_{halo} ratio with increasing

M^* , causing 2-armed morphologies to be favored at lower stellar concentrations at lower masses, 2) stellar mass growth being dominated by gas accretion in low mass galaxies, but by mergers in high mass galaxies, and 3) growth of the bulge at high galaxian masses due to mergers or other processes.

When comparing 2-armed galaxies at $z \sim 0.3$ and $z \sim 0.5$, for a given stellar mass we see larger concentrations at lower redshifts. Most of the observed difference in concentration can be accounted for by a morphological K-correction, plus lower effective resolution at higher redshifts. However, we cannot rule out that some of this apparent increase in concentration is caused by bulge growth over time. This result needs to be investigated further with larger sample sizes, better photometric redshifts, and detailed bulge/disk decompositions of the images.

We compare our Euclid arm count statistics with earlier statistics of the relative numbers of grand design, multi-armed, and flocculent galaxies determined by visual inspection of images by experts. We point out systematic selection effects in the samples, and discuss the need for better methods of quantifying spiral arm structure in galaxies.

Acknowledgements We thank Elena D’Onghia, Bruce Elmegreen, and the anonymous referee for helpful suggestions that greatly improved this paper. This research was supported by a grant from the NASA Tennessee Space Grant Consortium. This work has made use of the Euclid Q1 data from the Euclid mission of the European Space Agency (ESA) (European Space Agency & Euclid Consortium 2025). We thank the Euclid Consortium for making the Euclid Q1 catalogs available. The Euclid Consortium acknowledges the European Space Agency and a number of agencies and institutes that have supported the development of Euclid, in particular the Agenzia Spaziale Italiana, the Austrian Forschungsförderungsgesellschaft funded through BMK, the Belgian Science Policy, the Canadian Euclid Consortium, the Deutsches Zentrum für Luft- und Raumfahrt, the DTU Space and the Niels Bohr Institute in Denmark, the French Centre National d’Etudes Spatiales, the Fundação para a Ciência e a Tecnologia, the Hungarian Academy of Sciences, the Ministerio de Ciencia, Innovación y Universidades, the National Aeronautics and Space Administration, the National Astronomical Observatory of Japan, the Nederlandse Onderzoekschool Voor Astronomie, the Norwegian Space Agency, the Research Council of Finland, the Romanian Space Agency, the State Secretariat for Education, Research, and Innovation (SERI) at the Swiss Space Office (SSO), and the United Kingdom Space Agency. A complete and detailed list is available on the Euclid web site www.euclid-ec.org/

Facilities: Euclid(VIS)

Software: astropy (Astropy Collaboration et al. 2013, 2018, 2022)

REFERENCES

- Ann, H. B. 2014, Journal of Korean Astronomical Society, 47, 1, doi: [10.5303/JKAS.2014.47.1.1](https://doi.org/10.5303/JKAS.2014.47.1.1)
- Ann, H. B., & Lee, H.-R. 2013, Journal of Korean Astronomical Society, 46, 141, doi: [10.5303/JKAS.2013.46.3.141](https://doi.org/10.5303/JKAS.2013.46.3.141)
- Astropy Collaboration, Robitaille, T. P., Tollerud, E. J., et al. 2013, A&A, 558, A33, doi: [10.1051/0004-6361/201322068](https://doi.org/10.1051/0004-6361/201322068)
- Astropy Collaboration, Price-Whelan, A. M., Sipőcz, B. M., et al. 2018, AJ, 156, 123, doi: [10.3847/1538-3881/aabc4f](https://doi.org/10.3847/1538-3881/aabc4f)
- Astropy Collaboration, Price-Whelan, A. M., Lim, P. L., et al. 2022, ApJ, 935, 167, doi: [10.3847/1538-4357/ac7c74](https://doi.org/10.3847/1538-4357/ac7c74)
- Athanassoula, E. 1980, A&A, 88, 184
- . 2005, MNRAS, 358, 1477, doi: [10.1111/j.1365-2966.2005.08872.x](https://doi.org/10.1111/j.1365-2966.2005.08872.x)
- . 2012, MNRAS, 426, L46, doi: [10.1111/j.1745-3933.2012.01320.x](https://doi.org/10.1111/j.1745-3933.2012.01320.x)
- Baba, J., Saitoh, T. R., & Wada, K. 2013, ApJ, 763, 46, doi: [10.1088/0004-637X/763/1/46](https://doi.org/10.1088/0004-637X/763/1/46)
- Barro, G., Faber, S. M., Koo, D. C., et al. 2017, ApJ, 840, 47, doi: [10.3847/1538-4357/aa6b05](https://doi.org/10.3847/1538-4357/aa6b05)
- Behroozi, P. S., Conroy, C., & Wechsler, R. H. 2010, ApJ, 717, 379, doi: [10.1088/0004-637X/717/1/379](https://doi.org/10.1088/0004-637X/717/1/379)
- Bell, E. F., van der Wel, A., Papovich, C., et al. 2012, ApJ, 753, 167, doi: [10.1088/0004-637X/753/2/167](https://doi.org/10.1088/0004-637X/753/2/167)
- Bertin, G., Lin, C. C., Lowe, S. A., & Thurstans, R. P. 1989a, ApJ, 338, 78, doi: [10.1086/167182](https://doi.org/10.1086/167182)
- . 1989b, ApJ, 338, 104, doi: [10.1086/167183](https://doi.org/10.1086/167183)
- Birnboim, Y., & Dekel, A. 2003, MNRAS, 345, 349, doi: [10.1046/j.1365-8711.2003.06955.x](https://doi.org/10.1046/j.1365-8711.2003.06955.x)
- Bittner, A., Gadotti, D. A., Elmegreen, B. G., et al. 2017, MNRAS, 471, 1070, doi: [10.1093/mnras/stx1646](https://doi.org/10.1093/mnras/stx1646)
- Bland-Hawthorn, J., Tepper-Garcia, T., Agertz, O., & Federrath, C. 2024, ApJ, 968, 86, doi: [10.3847/1538-4357/ad4118](https://doi.org/10.3847/1538-4357/ad4118)
- Bouché, N., Dekel, A., Genzel, R., et al. 2010, ApJ, 718, 1001, doi: [10.1088/0004-637X/718/2/1001](https://doi.org/10.1088/0004-637X/718/2/1001)
- Bournaud, F., Dekel, A., Teyssier, R., et al. 2011, ApJL, 741, L33, doi: [10.1088/2041-8205/741/2/L33](https://doi.org/10.1088/2041-8205/741/2/L33)

- Buta, R. J., Sheth, K., Athanassoula, E., et al. 2015, *ApJS*, 217, 32, doi: [10.1088/0067-0049/217/2/32](https://doi.org/10.1088/0067-0049/217/2/32)
- Byrd, G. G., & Howard, S. 1992, *AJ*, 103, 1089, doi: [10.1086/116128](https://doi.org/10.1086/116128)
- Casteels, K. R. V., Bamford, S. P., Skibba, R. A., et al. 2013, *MNRAS*, 429, 1051, doi: [10.1093/mnras/sts391](https://doi.org/10.1093/mnras/sts391)
- Cattaneo, A., Dekel, A., Devriendt, J., Guiderdoni, B., & Blaizot, J. 2006, *MNRAS*, 370, 1651, doi: [10.1111/j.1365-2966.2006.10608.x](https://doi.org/10.1111/j.1365-2966.2006.10608.x)
- Cattaneo, A., Dimauro, P., & Koutsouridou, I. 2025, *MNRAS*, 537, 3929, doi: [10.1093/mnras/staf253](https://doi.org/10.1093/mnras/staf253)
- Chakrabarti, S., Laughlin, G., & Shu, F. H. 2003, *ApJ*, 596, 220, doi: [10.1086/377578](https://doi.org/10.1086/377578)
- Conselice, C. J. 2014, *ARA&A*, 52, 291, doi: [10.1146/annurev-astro-081913-040037](https://doi.org/10.1146/annurev-astro-081913-040037)
- Croton, D. J., Springel, V., White, S. D. M., et al. 2006, *MNRAS*, 365, 11, doi: [10.1111/j.1365-2966.2005.09675.x](https://doi.org/10.1111/j.1365-2966.2005.09675.x)
- de Vaucouleurs, G., de Vaucouleurs, A., & Corwin, J. R. 1976, Second reference catalogue of bright galaxies, 1976, 0
- Dekel, A., & Birnboim, Y. 2006, *MNRAS*, 368, 2, doi: [10.1111/j.1365-2966.2006.10145.x](https://doi.org/10.1111/j.1365-2966.2006.10145.x)
- Dekel, A., & Burkert, A. 2014, *MNRAS*, 438, 1870, doi: [10.1093/mnras/stt2331](https://doi.org/10.1093/mnras/stt2331)
- Dekel, A., Sari, R., & Ceverino, D. 2009, *ApJ*, 703, 785, doi: [10.1088/0004-637X/703/1/785](https://doi.org/10.1088/0004-637X/703/1/785)
- Dekel, A., & Woo, J. 2003, *MNRAS*, 344, 1131, doi: [10.1046/j.1365-8711.2003.06923.x](https://doi.org/10.1046/j.1365-8711.2003.06923.x)
- DESI Collaboration: Abdul-Karim, M., Adame, A. G., Aguado, D., et al. 2025, arXiv e-prints, arXiv:2503.14745, doi: [10.48550/arXiv.2503.14745](https://doi.org/10.48550/arXiv.2503.14745)
- Díaz-García, S., Salo, H., Knapen, J. H., & Herrera-Endoqui, M. 2019, *A&A*, 631, A94, doi: [10.1051/0004-6361/201936000](https://doi.org/10.1051/0004-6361/201936000)
- Dobbs, C., & Baba, J. 2014, *PASA*, 31, e035, doi: [10.1017/pasa.2014.31](https://doi.org/10.1017/pasa.2014.31)
- Dobbs, C. L., Pettitt, A. R., Corbelli, E., & Pringle, J. E. 2018, *MNRAS*, 478, 3793, doi: [10.1093/mnras/sty1231](https://doi.org/10.1093/mnras/sty1231)
- Dobbs, C. L., Theis, C., Pringle, J. E., & Bate, M. R. 2010, *MNRAS*, 403, 625, doi: [10.1111/j.1365-2966.2009.16161.x](https://doi.org/10.1111/j.1365-2966.2009.16161.x)
- D'Onghia, E. 2015, *ApJL*, 808, L8, doi: [10.1088/2041-8205/808/1/L8](https://doi.org/10.1088/2041-8205/808/1/L8)
- D'Onghia, E., Vogelsberger, M., & Hernquist, L. 2013, *ApJ*, 766, 34, doi: [10.1088/0004-637X/766/1/34](https://doi.org/10.1088/0004-637X/766/1/34)
- Durbala, A., Buta, R., Sulentic, J. W., & Verdes-Montenegro, L. 2009, *MNRAS*, 397, 1756, doi: [10.1111/j.1365-2966.2009.15051.x](https://doi.org/10.1111/j.1365-2966.2009.15051.x)
- Elmegreen, B. G. 2002, *ApJ*, 577, 206, doi: [10.1086/342177](https://doi.org/10.1086/342177)
- Elmegreen, B. G., & Elmegreen, D. M. 1986, *ApJ*, 311, 554, doi: [10.1086/164795](https://doi.org/10.1086/164795)
- Elmegreen, D. M., & Elmegreen, B. G. 1982, *MNRAS*, 201, 1021, doi: [10.1093/mnras/201.4.1021](https://doi.org/10.1093/mnras/201.4.1021)
- . 1987, *ApJ*, 314, 3, doi: [10.1086/165034](https://doi.org/10.1086/165034)
- . 1995, *ApJ*, 445, 591, doi: [10.1086/175723](https://doi.org/10.1086/175723)
- Elmegreen, D. M., Elmegreen, B. G., Yau, A., et al. 2011, *ApJ*, 737, 32, doi: [10.1088/0004-637X/737/1/32](https://doi.org/10.1088/0004-637X/737/1/32)
- Espejo Salcedo, J. M., Pastras, S., Vácha, J., et al. 2025, *A&A*, 700, A42, doi: [10.1051/0004-6361/202554725](https://doi.org/10.1051/0004-6361/202554725)
- Euclid Collaboration: Aussel, H., Tereno, I., Schirmer, M., et al. 2025, arXiv e-prints, arXiv:2503.15302, doi: [10.48550/arXiv.2503.15302](https://doi.org/10.48550/arXiv.2503.15302)
- Euclid Collaboration: Cropper, M. S., Al-Bahlawan, A., Amiaux, J., et al. 2025, *A&A*, 697, A2, doi: [10.1051/0004-6361/202450996](https://doi.org/10.1051/0004-6361/202450996)
- Euclid Collaboration: Desprez, G., Paltani, S., Coupon, J., et al. 2020, *A&A*, 644, A31, doi: [10.1051/0004-6361/202039403](https://doi.org/10.1051/0004-6361/202039403)
- Euclid Collaboration: Enia, A., Pozzetti, L., Bolzonella, M., et al. 2025, arXiv e-prints, arXiv:2503.15314, doi: [10.48550/arXiv.2503.15314](https://doi.org/10.48550/arXiv.2503.15314)
- Euclid Collaboration: Gentile, F., Daddi, E., Elbaz, D., et al. 2025, arXiv e-prints, arXiv:2511.02964, doi: [10.48550/arXiv.2511.02964](https://doi.org/10.48550/arXiv.2511.02964)
- Euclid Collaboration: Mellier, Y., Abdurro'uf, Acevedo Barroso, J. A., et al. 2025, *A&A*, 697, A1, doi: [10.1051/0004-6361/202450810](https://doi.org/10.1051/0004-6361/202450810)
- Euclid Collaboration: Quilley, L., Damjanov, I., de Lapparent, V., et al. 2025, arXiv e-prints, arXiv:2503.15309, doi: [10.48550/arXiv.2503.15309](https://doi.org/10.48550/arXiv.2503.15309)
- Euclid Collaboration: Romelli, E., Kümmel, M., Dole, H., et al. 2025, arXiv e-prints, arXiv:2503.15305, doi: [10.48550/arXiv.2503.15305](https://doi.org/10.48550/arXiv.2503.15305)
- Euclid Collaboration: Tucci, M., Paltani, S., Hartley, W. G., et al. 2025, arXiv e-prints, arXiv:2503.15306, doi: [10.48550/arXiv.2503.15306](https://doi.org/10.48550/arXiv.2503.15306)
- Euclid Collaboration: Walmsley, M., Huertas-Company, M., Quilley, L., et al. 2025, arXiv e-prints, arXiv:2503.15310, doi: [10.48550/arXiv.2503.15310](https://doi.org/10.48550/arXiv.2503.15310)
- European Space Agency, & Euclid Consortium. 2025, Euclid Quick Release (Q1), European Space Agency, doi: [10.57780/ESA-2853F3B](https://doi.org/10.57780/ESA-2853F3B). <http://esdcdoid.esac.esa.int/doi/html/data/astronomy/euclid/eqrq1.html>
- Ferrarese, L., & Merritt, D. 2000, *ApJL*, 539, L9, doi: [10.1086/312838](https://doi.org/10.1086/312838)
- Fraser-McKelvie, A., Brown, M. J. I., Pimblet, K., Dolley, T., & Bonne, N. J. 2018, *MNRAS*, 474, 1909, doi: [10.1093/mnras/stx2823](https://doi.org/10.1093/mnras/stx2823)
- Fujii, M. S., Bédorf, J., Baba, J., & Portegies Zwart, S. 2018, *MNRAS*, 477, 1451, doi: [10.1093/mnras/sty711](https://doi.org/10.1093/mnras/sty711)

- Gao, H., Ho, L. C., Barth, A. J., & Li, Z.-Y. 2020, *ApJS*, 247, 20, doi: [10.3847/1538-4365/ab67b2](https://doi.org/10.3847/1538-4365/ab67b2)
- Gao, H., Ho, L. C., & Li, Z.-Y. 2022, *ApJS*, 262, 54, doi: [10.3847/1538-4365/ac8dea](https://doi.org/10.3847/1538-4365/ac8dea)
- Garofalo, D., North, M., Belga, L., & Waddell, K. 2020, *ApJ*, 890, 144, doi: [10.3847/1538-4357/ab6f70](https://doi.org/10.3847/1538-4357/ab6f70)
- Ghosh, S., & D’Onghia, E. 2025, arXiv e-prints, arXiv:2510.25848, doi: [10.48550/arXiv.2510.25848](https://doi.org/10.48550/arXiv.2510.25848)
- Girelli, G., Pozzetti, L., Bolzonella, M., et al. 2020, *A&A*, 634, A135, doi: [10.1051/0004-6361/201936329](https://doi.org/10.1051/0004-6361/201936329)
- Goldreich, P., & Lynden-Bell, D. 1965, *MNRAS*, 130, 125, doi: [10.1093/mnras/130.2.125](https://doi.org/10.1093/mnras/130.2.125)
- Goto, T., Yamauchi, C., Fujita, Y., et al. 2003, *MNRAS*, 346, 601, doi: [10.1046/j.1365-2966.2003.07114.x](https://doi.org/10.1046/j.1365-2966.2003.07114.x)
- Graham, A. W., & Driver, S. P. 2005, *PASA*, 22, 118, doi: [10.1071/AS05001](https://doi.org/10.1071/AS05001)
- Grand, R. J. J., Kawata, D., & Cropper, M. 2013, *A&A*, 553, A77, doi: [10.1051/0004-6361/201321308](https://doi.org/10.1051/0004-6361/201321308)
- Grosbøl, P., Patsis, P. A., & Pompei, E. 2004, *A&A*, 423, 849, doi: [10.1051/0004-6361:20035804](https://doi.org/10.1051/0004-6361:20035804)
- Hart, R. E., Bamford, S. P., Casteels, K. R. V., et al. 2017a, *MNRAS*, 468, 1850, doi: [10.1093/mnras/stx581](https://doi.org/10.1093/mnras/stx581)
- Hart, R. E., Bamford, S. P., Willett, K. W., et al. 2016, *MNRAS*, 461, 3663, doi: [10.1093/mnras/stw1588](https://doi.org/10.1093/mnras/stw1588)
- Hart, R. E., Bamford, S. P., Hayes, W. B., et al. 2017b, *MNRAS*, 472, 2263, doi: [10.1093/mnras/stx2137](https://doi.org/10.1093/mnras/stx2137)
- Hopkins, P. F., Bundy, K., Croton, D., et al. 2010, *ApJ*, 715, 202, doi: [10.1088/0004-637X/715/1/202](https://doi.org/10.1088/0004-637X/715/1/202)
- Howard, S., Keel, W. C., Byrd, G., & Burkey, J. 1993, *ApJ*, 417, 502, doi: [10.1086/173329](https://doi.org/10.1086/173329)
- Julian, W. H., & Toomre, A. 1966, *ApJ*, 146, 810, doi: [10.1086/148957](https://doi.org/10.1086/148957)
- Kent, S. M. 1985, *ApJS*, 59, 115, doi: [10.1086/191066](https://doi.org/10.1086/191066)
- Kereš, D., Katz, N., Weinberg, D. H., & Davé, R. 2005, *MNRAS*, 363, 2, doi: [10.1111/j.1365-2966.2005.09451.x](https://doi.org/10.1111/j.1365-2966.2005.09451.x)
- King, A. 2003, *ApJL*, 596, L27, doi: [10.1086/379143](https://doi.org/10.1086/379143)
- Kong, D., Xu, Y., Liu, D., et al. 2025, *AJ*, 170, 243, doi: [10.3847/1538-3881/ae0320](https://doi.org/10.3847/1538-3881/ae0320)
- Kormendy, J., & Kennicutt, Jr., R. C. 2004, *ARA&A*, 42, 603, doi: [10.1146/annurev.astro.42.053102.134024](https://doi.org/10.1146/annurev.astro.42.053102.134024)
- Kormendy, J., & Norman, C. A. 1979, *ApJ*, 233, 539, doi: [10.1086/157414](https://doi.org/10.1086/157414)
- Kuhn, V., Guo, Y., Martin, A., et al. 2024, *ApJL*, 968, L15, doi: [10.3847/2041-8213/ad43eb](https://doi.org/10.3847/2041-8213/ad43eb)
- Lelli, F., McGaugh, S. S., Schombert, J. M., & Pawlowski, M. S. 2016, *ApJL*, 827, L19, doi: [10.3847/2041-8205/827/1/L19](https://doi.org/10.3847/2041-8205/827/1/L19)
- Lin, C. C., & Bertin, G. 1985, in *IAU Symposium*, Vol. 106, *The Milky Way Galaxy*, ed. H. van Woerden, R. J. Allen, & W. B. Burton, 513–530
- Lin, C. C., & Shu, F. H. 1964, *ApJ*, 140, 646, doi: [10.1086/147955](https://doi.org/10.1086/147955)
- . 1966, *Proceedings of the National Academy of Science*, 55, 229, doi: [10.1073/pnas.55.2.229](https://doi.org/10.1073/pnas.55.2.229)
- Luo, Y., Faber, S. M., Rodríguez-Puebla, A., et al. 2020, *MNRAS*, 493, 1686, doi: [10.1093/mnras/staa328](https://doi.org/10.1093/mnras/staa328)
- Margalef-Bentabol, B., Conselice, C. J., Haeussler, B., et al. 2022, *MNRAS*, 511, 1502, doi: [10.1093/mnras/stac080](https://doi.org/10.1093/mnras/stac080)
- Marleau, F. R., Habas, R., Carollo, D., et al. 2025, arXiv e-prints, arXiv:2503.15335, doi: [10.48550/arXiv.2503.15335](https://doi.org/10.48550/arXiv.2503.15335)
- Martig, M., Bournaud, F., Teyssier, R., & Dekel, A. 2009, *ApJ*, 707, 250, doi: [10.1088/0004-637X/707/1/250](https://doi.org/10.1088/0004-637X/707/1/250)
- Martinsson, T. P. K., Verheijen, M. A. W., Westfall, K. B., et al. 2013, *A&A*, 557, A131, doi: [10.1051/0004-6361/201321390](https://doi.org/10.1051/0004-6361/201321390)
- Masters, K. L., Mosleh, M., Romer, A. K., et al. 2010, *MNRAS*, 405, 783, doi: [10.1111/j.1365-2966.2010.16503.x](https://doi.org/10.1111/j.1365-2966.2010.16503.x)
- Méndez-Abreu, J., de Lorenzo-Cáceres, A., & Sánchez, S. F. 2021, *MNRAS*, 504, 3058, doi: [10.1093/mnras/stab1064](https://doi.org/10.1093/mnras/stab1064)
- Metcalfe, R. B., & Magliocchetti, M. 2006, *MNRAS*, 365, 101, doi: [10.1111/j.1365-2966.2005.09649.x](https://doi.org/10.1111/j.1365-2966.2005.09649.x)
- Michikoshi, S., & Kokubo, E. 2018, *MNRAS*, 481, 185, doi: [10.1093/mnras/sty2274](https://doi.org/10.1093/mnras/sty2274)
- Minniti, J. H., Zoccali, M., Rojas-Arriagada, A., et al. 2021, *A&A*, 654, A138, doi: [10.1051/0004-6361/202039512](https://doi.org/10.1051/0004-6361/202039512)
- Neumann, J., Wisotzki, L., Choudhury, O. S., et al. 2017, *A&A*, 604, A30, doi: [10.1051/0004-6361/201730601](https://doi.org/10.1051/0004-6361/201730601)
- Noeske, K. G., Weiner, B. J., Faber, S. M., et al. 2007, *ApJL*, 660, L43, doi: [10.1086/517926](https://doi.org/10.1086/517926)
- Oh, S. H., Kim, W.-T., & Lee, H. M. 2015, *ApJ*, 807, 73, doi: [10.1088/0004-637X/807/1/73](https://doi.org/10.1088/0004-637X/807/1/73)
- Oh, S. H., Kim, W.-T., Lee, H. M., & Kim, J. 2008, *ApJ*, 683, 94, doi: [10.1086/588184](https://doi.org/10.1086/588184)
- Papovich, C., Labbé, I., Quadri, R., et al. 2015, *ApJ*, 803, 26, doi: [10.1088/0004-637X/803/1/26](https://doi.org/10.1088/0004-637X/803/1/26)
- Patsis, P. A., Grosbøl, P., & Hiortelid, N. 1997, *A&A*, 323, 762
- Patsis, P. A., & Okalidis, P. 2025, *Galaxies*, 13, 132, doi: [10.3390/galaxies13060132](https://doi.org/10.3390/galaxies13060132)
- Planck Collaboration: Ade, P. A. R., Aghanim, N., Arnaud, M., et al. 2016, *A&A*, 594, A13, doi: [10.1051/0004-6361/201525830](https://doi.org/10.1051/0004-6361/201525830)
- Ponomareva, A. A., Mancera Piña, P. E., Vărașteanu, A. A., et al. 2026, *MNRAS*, 548, stag531, doi: [10.1093/mnras/stag531](https://doi.org/10.1093/mnras/stag531)
- Popesso, P., Concas, A., Cresci, G., et al. 2023, *MNRAS*, 519, 1526, doi: [10.1093/mnras/stac3214](https://doi.org/10.1093/mnras/stac3214)

- Quinn, J. R., Loebman, S. R., Daniel, K. J., et al. 2025, arXiv e-prints, arXiv:2507.22793, doi: [10.48550/arXiv.2507.22793](https://doi.org/10.48550/arXiv.2507.22793)
- Reid, M. J., Menten, K. M., Brunthaler, A., et al. 2019, ApJ, 885, 131, doi: [10.3847/1538-4357/ab4a11](https://doi.org/10.3847/1538-4357/ab4a11)
- Sachdeva, S., Gadotti, D. A., Saha, K., & Singh, H. P. 2015, MNRAS, 451, 2, doi: [10.1093/mnras/stv931](https://doi.org/10.1093/mnras/stv931)
- Sachdeva, S., Saha, K., & Singh, H. P. 2017, ApJ, 840, 79, doi: [10.3847/1538-4357/aa6c61](https://doi.org/10.3847/1538-4357/aa6c61)
- Saha, B., Dutta, S., & Banerjee, A. 2025, ApJ, 991, 63, doi: [10.3847/1538-4357/adf840](https://doi.org/10.3847/1538-4357/adf840)
- Saha, K., & Elmegreen, B. 2016, ApJL, 826, L21, doi: [10.3847/2041-8205/826/2/L21](https://doi.org/10.3847/2041-8205/826/2/L21)
- Salim, S., Rich, R. M., Charlot, S., et al. 2007, ApJS, 173, 267, doi: [10.1086/519218](https://doi.org/10.1086/519218)
- Salim, S., Lee, J. C., Janowiecki, S., et al. 2016, ApJS, 227, 2, doi: [10.3847/0067-0049/227/1/2](https://doi.org/10.3847/0067-0049/227/1/2)
- Salo, H., Laurikainen, E., Buta, R., & Knapen, J. H. 2010, ApJL, 715, L56, doi: [10.1088/2041-8205/715/1/L56](https://doi.org/10.1088/2041-8205/715/1/L56)
- Sanders, R. H., & Huntley, J. M. 1976, ApJ, 209, 53, doi: [10.1086/154692](https://doi.org/10.1086/154692)
- Sazonova, E., Morgan, C. R., Balogh, M., et al. 2025, arXiv e-prints, arXiv:2511.09644, doi: [10.48550/arXiv.2511.09644](https://doi.org/10.48550/arXiv.2511.09644)
- Schiminovich, D., Wyder, T. K., Martin, D. C., et al. 2007, ApJS, 173, 315, doi: [10.1086/524659](https://doi.org/10.1086/524659)
- Sellwood, J. A. 2012, ApJ, 751, 44, doi: [10.1088/0004-637X/751/1/44](https://doi.org/10.1088/0004-637X/751/1/44)
- . 2014, Reviews of Modern Physics, 86, 1, doi: [10.1103/RevModPhys.86.1](https://doi.org/10.1103/RevModPhys.86.1)
- Shu, F. H. 2016, ARA&A, 54, 667, doi: [10.1146/annurev-astro-081915-023426](https://doi.org/10.1146/annurev-astro-081915-023426)
- Smith, B. J., Giroux, M. L., & Struck, C. 2022, AJ, 164, 146, doi: [10.3847/1538-3881/ac88c5](https://doi.org/10.3847/1538-3881/ac88c5)
- Smith, B. J., Watson, M., Giroux, M. L., & Struck, C. 2024, AJ, 168, 12, doi: [10.3847/1538-3881/ad46fb](https://doi.org/10.3847/1538-3881/ad46fb)
- Somerville, R. S., Hopkins, P. F., Cox, T. J., Robertson, B. E., & Hernquist, L. 2008, MNRAS, 391, 481, doi: [10.1111/j.1365-2966.2008.13805.x](https://doi.org/10.1111/j.1365-2966.2008.13805.x)
- Speagle, J. S., Steinhardt, C. L., Capak, P. L., & Silverman, J. D. 2014, ApJS, 214, 15, doi: [10.1088/0067-0049/214/2/15](https://doi.org/10.1088/0067-0049/214/2/15)
- Starkman, N., Lelli, F., McGaugh, S., & Schombert, J. 2018, MNRAS, 480, 2292, doi: [10.1093/mnras/sty2011](https://doi.org/10.1093/mnras/sty2011)
- Struck, C., Dobbs, C. L., & Hwang, J.-S. 2011, MNRAS, 414, 2498, doi: [10.1111/j.1365-2966.2011.18568.x](https://doi.org/10.1111/j.1365-2966.2011.18568.x)
- Tacchella, S., Diemer, B., Hernquist, L., et al. 2019, MNRAS, 487, 5416, doi: [10.1093/mnras/stz1657](https://doi.org/10.1093/mnras/stz1657)
- Tasca, L. A. M., Tresse, L., Le Fèvre, O., et al. 2014, A&A, 564, L12, doi: [10.1051/0004-6361/201423699](https://doi.org/10.1051/0004-6361/201423699)
- Taylor-Mager, V. A., Conselice, C. J., Windhorst, R. A., & Jansen, R. A. 2007, ApJ, 659, 162, doi: [10.1086/511806](https://doi.org/10.1086/511806)
- Thomasson, M., Donner, K. J., Sundelius, B., et al. 1989, A&A, 211, 25
- Thorp, M. D., Bluck, A. F. L., Ellison, S. L., et al. 2021, MNRAS, 507, 886, doi: [10.1093/mnras/stab2201](https://doi.org/10.1093/mnras/stab2201)
- Toomre, A., & Toomre, J. 1972, ApJ, 178, 623, doi: [10.1086/151823](https://doi.org/10.1086/151823)
- Vallée, J. P. 2016, AJ, 151, 55, doi: [10.3847/0004-6256/151/3/55](https://doi.org/10.3847/0004-6256/151/3/55)
- van Albada, T. S., Bahcall, J. N., Begeman, K., & Sancisi, R. 1985, ApJ, 295, 305, doi: [10.1086/163375](https://doi.org/10.1086/163375)
- van der Wel, A., Franx, M., van Dokkum, P. G., et al. 2014, ApJ, 788, 28, doi: [10.1088/0004-637X/788/1/28](https://doi.org/10.1088/0004-637X/788/1/28)
- van Dokkum, P. G., Whitaker, K. E., Brammer, G., et al. 2010, ApJ, 709, 1018, doi: [10.1088/0004-637X/709/2/1018](https://doi.org/10.1088/0004-637X/709/2/1018)
- Walmsley, M., Huertas-Company, M., Quilley, L., et al. 2025, Euclid Quick Data Release (Q1): First visual morphology catalogue, Zenodo, doi: [10.5281/zenodo.15106473](https://doi.org/10.5281/zenodo.15106473), [https://doi.org/10.5281/zenodo.15106473](https://doi.org/https://doi.org/10.5281/zenodo.15106473)
- Wang, J.-H., Li, Z.-Y., Zhuang, M.-Y., Ho, L. C., & Lai, L.-M. 2024, A&A, 686, A100, doi: [10.1051/0004-6361/202348934](https://doi.org/10.1051/0004-6361/202348934)
- Wei, J., Xu, Y., Lin, Z., et al. 2024, AJ, 168, 264, doi: [10.3847/1538-3881/ad8632](https://doi.org/10.3847/1538-3881/ad8632)
- Weinmann, S. M., Kauffmann, G., van den Bosch, F. C., et al. 2009, MNRAS, 394, 1213, doi: [10.1111/j.1365-2966.2009.14412.x](https://doi.org/10.1111/j.1365-2966.2009.14412.x)
- Whitney, A., Ferreira, L., Conselice, C. J., & Duncan, K. 2021, ApJ, 919, 139, doi: [10.3847/1538-4357/ac1422](https://doi.org/10.3847/1538-4357/ac1422)
- Willett, K. W., Lintott, C. J., Bamford, S. P., et al. 2013, MNRAS, 435, 2835, doi: [10.1093/mnras/stt1458](https://doi.org/10.1093/mnras/stt1458)
- Willett, K. W., Schawinski, K., Simmons, B. D., et al. 2015, MNRAS, 449, 820, doi: [10.1093/mnras/stv307](https://doi.org/10.1093/mnras/stv307)
- Wuyts, S., Förster Schreiber, N. M., van der Wel, A., et al. 2011, ApJ, 742, 96, doi: [10.1088/0004-637X/742/2/96](https://doi.org/10.1088/0004-637X/742/2/96)
- Xu, Y., Hao, C. J., Liu, D. J., et al. 2023, ApJ, 947, 54, doi: [10.3847/1538-4357/acc45c](https://doi.org/10.3847/1538-4357/acc45c)
- Yeoun-Gyu Choi, I., & Ann, H. B. 2011, Journal of Korean Astronomical Society, 44, 161, doi: [10.5303/JKAS.2011.44.5.161](https://doi.org/10.5303/JKAS.2011.44.5.161)
- Yu, S.-Y., Cheng, C., Pan, Y., Sun, F., & Li, Y. A. 2023, A&A, 676, A74, doi: [10.1051/0004-6361/202346140](https://doi.org/10.1051/0004-6361/202346140)
- Yu, S.-Y., & Ho, L. C. 2020, ApJ, 900, 150, doi: [10.3847/1538-4357/abac5b](https://doi.org/10.3847/1538-4357/abac5b)
- Yu, S.-Y., Ho, L. C., Barth, A. J., & Li, Z.-Y. 2018, ApJ, 862, 13, doi: [10.3847/1538-4357/aacb25](https://doi.org/10.3847/1538-4357/aacb25)

Zolotov, A., Dekel, A., Mandelker, N., et al. 2015, MNRAS, 450, 2327, doi: [10.1093/mnras/stv740](https://doi.org/10.1093/mnras/stv740)